Towards A Unified Min-Max Framework for Adversarial Exploration and Robustness

Anonymous authors
Paper under double-blind review

Abstract

The worst-case training principle that minimizes the maximal adversarial loss, also known as adversarial training (AT), has shown to be a state-of-the-art approach for enhancing adversarial robustness against norm-ball bounded input perturbations. Nonetheless, min-max optimization beyond the purpose of AT has not been rigorously explored in the research of adversarial attack and defense. In particular, given a set of risk sources (domains), minimizing the maximal loss induced from the domain set can be reformulated as a general min-max problem that is fundamentally different from AT since the maximization is taken over the probability simplex of the domain set. Examples of this general formulation include attacking model ensembles, devising universal perturbation under multiple inputs or data transformations, and generalized AT over different types of attack models. We show that these problems can be solved under a unified and theoretically principled min-max optimization framework. We also show that the self-adjusted domain weights learnt from our method provide a holistic tool to explain the difficulty level of attack and defense over multiple domains. Extensive experiments show that our approach leads to substantial performance improvement over the conventional heuristic strategies[1].

1 Introduction

Training a machine learning model that is capable of assuring its worst-case performance against all possible adversaries given a specified threat model is a fundamental yet challenging problem, especially for deep neural networks (DNNs) (Szegedy et al., 2013; Goodfellow et al., 2015; Carlini & Wagner, 2017). A common practice to train an adversarially robust model is based on a specific form of min-max training, known as *adversarial training* (AT) (Goodfellow et al., 2015; Madry et al., 2017), where the minimization step learns model weights under the adversarial loss constructed at the maximization step in an alternative training fashion. On datasets such as MNIST and CIFAR-10, AT has achieved the state-of-the-art defense performance against ℓ_p-norm-ball input perturbations (Athalye et al., 2018b).

Motivated by the success of AT, one follow-up question that naturally arises is: *Beyond AT, can other types of min-max formulation and optimization techniques advance the research in adversarial robustness?* In this paper, we give an affirmative answer corroborated by the substantial performance gain and the ability of self-learned risk interpretation using our proposed min-max framework on several tasks for adversarial attack and defense.

We demonstrate the utility of a general formulation for min-max optimization minimizing the maximal loss induced from a set of risk sources (domains). Our considered min-max formulation is fundamentally different from AT, as our maximization step is taken over the probability simplex of the set of domains. Moreover, we show that many problem setups in adversarial attacks and defenses can in fact be reformulated under this general min-max framework, including attacking model ensembles (Tramèr et al., 2018; Liu et al., 2018), devising universal perturbation to input samples (Moosavi-Dezfooli et al., 2017) or data transformations (Athalye & Sutskever, 2018; Brown et al., 2017), and generalized AT over multiple types of threat models (Tramèr & Boneh, 2019; Araujo et al., 2019). However, current methods for solving these tasks often rely on simple heuristics (e.g.,

---

[1] For reproducibility, the code and trained models will be released accompanying this paper.

uniform averaging), resulting in significant performance drops when comparing to our proposed min-max optimization framework.

Specifically, based on the general min-max framework, we show that these problems can be solved under the same optimization procedure and prove the rate of its algorithmic convergence. As a byproduct and an exclusive feature, by tracking the weighting factor associated with the probability simplex during training, our method can provide tools for self-adjusted risk assessment and obtain novel insights on the set of domains for the associated tasks.

Contributions   (1) We indicate the utility of min-max optimization beyond AT by proposing a general and theoretically grounded framework on adversarial attack and defense. (2) We demonstrate the effectiveness of our min-max framework by evaluating the proposed APGD attack on MNIST and CIFAR-10. In theory, we show that APGD has an $O(1/T)$ convergence rate, where T is the number of iterations. In practice, we show that APGD obtains 17.48%, 35.21% and 9.39% improvement on average compared with PGD attack on CIFAR-10. (3) We propose a generalized AT scheme under mixed types of adversarial attacks and demonstrate that the diversified attack ensemble helps adversarial robustness. Compared with vanilla AT, our new training scheme leads to better worst-case robustness even if the defender lacks prior knowledge of the strengths of attacks. (4) We show how the weighting factors of the probability simplex help to obtain novel insights for associated tasks and interpreting the importance of candidates in domains.

Related Work   Recent studies have identified that DNNs are highly vulnerable to adversarial manipulations in various applications (Szegedy et al., 2013; Carlini et al., 2016; Jia & Liang, 2017; Lin et al., 2017; Huang et al., 2017; Carlini & Wagner, 2018; Zhao et al., 2018; Eykholt et al., 2018; Chen et al., 2018a; Lei et al., 2019), thus leading to an arms race between adversarial attacks (Carlini & Wagner, 2017; Athalye et al., 2018b; Goodfellow et al., 2014; Papernot et al., 2016a; Moosavi Dezfooli et al., 2016; Chen et al., 2018b; Xu et al., 2019) and defenses (Madry et al., 2017; Papernot et al., 2016b; Meng & Chen, 2017; Xie et al., 2017; Xu et al., 2018). One intriguing property of adversarial examples is the transferability across multiple domains (Liu et al., 2017; Tramèr et al., 2017; Papernot et al., 2017; Su et al., 2018), which indicates a more challenging yet promising research direction – devising universal adversarial perturbations over model ensembles (Tramèr et al., 2018; Liu et al., 2018), input samples (Moosavi-Dezfooli et al., 2017; Metzen et al., 2017; Shafahi et al., 2018) and data transformations (Athalye et al., 2018b; Athalye & Sutskever, 2018; Brown et al., 2017). However, current approaches suffer from a significant performance loss for resting on the uniform averaging strategy. We will compare these works with our min-max method in Sec. 4. As a natural extension following min-max attack, we study the generalized AT under multiple perturbations (Tramèr & Boneh, 2019; Araujo et al., 2019; Kang et al., 2019; Croce & Hein, 2019). Finally, our min-max framework is adapted and inspired by previous literature on robust learning over multiple domains (Qian et al., 2018; Rafique et al., 2018; Lu et al., 2018; 2019a).

2   Min-Max Power in Adversarial Exploration and Robustness

We begin by introducing the principle of robust learning over multiple domains and its connection to a specialized form of min-max optimization. We then show that the resulting min-max formulation fits into various attack settings for *adversarial exploration*: a) ensemble adversarial attack, b) universal adversarial perturbation and c) robust perturbation over data transformations. Finally, we propose a generalized adversarial training (AT) framework under mixed types of adversarial attacks to improve *model robustness*.

2.1   General idea: Robust learning over multiple domains

Consider K loss functions $\{F_i(\mathbf{v})\}$ (each of which is defined on a learning domain), the problem of robust learning over K domains can be formulated as (Qian et al., 2018; Rafique et al., 2018; Lu et al., 2018)

$$\underset{\mathbf{v}\in\mathcal{V}}{\text{minimize}}\ \underset{\mathbf{w}\in\mathcal{P}}{\text{maximize}}\quad \sum_{i=1}^{K} w_i F_i(\mathbf{v}), \tag{1}$$

where $\mathbf{v}$ and $\mathbf{w}$ are optimization variables, $\mathcal{V}$ is a constraint set, and $\mathcal{P}$ denotes the probability simplex $\mathcal{P} = \{\mathbf{w} \,|\, \mathbf{1}^T\mathbf{w} = 1, w_i \in [0, 1], \forall i\}$. Since the inner maximization problem in (1) is a linear function

of $\mathbf{w}$ over the probabilistic simplex, problem (1) is thus equivalent to

$$\operatorname*{minimize}_{\mathbf{v} \in \mathcal{V}} \operatorname*{maximize}_{i \in [K]} \quad F_i(\mathbf{v}), \tag{2}$$

where $[K]$ denotes the integer set $\{1, 2, \ldots, K\}$.

Benefit and computation challenge of (1)   Compared to multi-task learning in a finite-sum formulation which minimizes K losses on *average*, problem (1) provides consistently robust *worst-case* performance across all domains. This can be explained from the epigraph form of (2),

$$\operatorname*{minimize}_{\mathbf{v} \in \mathcal{V}, t} \ t, \quad \text{subject to } F_i(\mathbf{v}) \leq t, i \in [K], \tag{3}$$

where t is an epigraph variable (Boyd & Vandenberghe, 2004) that provides the t-level robustness at each domain.

Although the min-max problem (1) offers a great robustness interpretation as in (3), solving it becomes more challenging than solving the finite-sum problem. It is clear from (2) that the inner maximization problem of (1) always returns the one-hot value of $\mathbf{w}$, namely, $\mathbf{w} = \mathbf{e}_i$, where $\mathbf{e}_i$ is the ith standard basis vector, and $i = \arg\max_i \{F_i(\mathbf{v})\}$. The one-hot coding reduces the generalizability to other domains and induces instability of the learning procedure in practice. Such an issue is often mitigated by introducing a strongly concave regularizer in the inner maximization step (Lu et al., 2018; Qian et al., 2018).

Regularized problem formulation   Spurred by (Qian et al., 2018), we penalize the distance between the *worst-case* loss and the *average* loss over K domains. This yields

$$\operatorname*{minimize}_{\mathbf{v} \in \mathcal{V}} \operatorname*{maximize}_{\mathbf{w} \in \mathcal{P}} \quad \sum_{i=1}^{K} w_i F_i(\mathbf{v}) - \tfrac{\gamma}{2} \|\mathbf{w} - \mathbf{1}/K\|_2^2, \tag{4}$$

where $\gamma > 0$ is a regularization parameter. As $\gamma \to 0$, problem (4) is equivalent to (1). By contrast, it becomes the finite-sum problem when $\gamma \to \infty$ since $\mathbf{w} \to \mathbf{1}/K$. *In this sense, the trainable* $\mathbf{w}$ *provides an essential indicator on the importance level of each domain.* The larger the weight is, the more important the domain is. We call $\mathbf{w}$ *domain weights* in this paper. We next show how the principle of robust learning over multiple domains can fit into various settings of adversarial attack and defense problems.

2.2   Robust adversarial attacks

The general goal of adversarial attack is to craft an adversarial example $\mathbf{x}' = \mathbf{x}_0 + \boldsymbol{\delta} \in \mathbb{R}^d$ to mislead the prediction of machine learning (ML) or deep learning (DL) systems, where $\mathbf{x}_0$ denotes the natural example with the true label t_0, and $\boldsymbol{\delta}$ is known as *adversarial perturbation*, commonly subject to ℓ_p-norm ($p \in \{0, 1, 2, \infty\}$) constraint $\mathcal{X} := \{\boldsymbol{\delta} \,|\, \|\boldsymbol{\delta}\|_p \leq \epsilon, \ \mathbf{x}_0 + \boldsymbol{\delta} \in [0, 1]^d\}$ for a given small number ϵ. Here the ℓ_p norm enforces the similarity between $\mathbf{x}'$ and $\mathbf{x}_0$, and the input space of ML/DL systems is normalized to $[0, 1]^d$.

Ensemble attack over multiple models   Consider K ML/DL models $\{\mathcal{M}_i\}_{i=1}^{K}$, the goal is to find robust adversarial examples that can fool all K models simultaneously. In this case, the notion of 'domain' in (4) is specified as 'model', and the objective function F_i in (4) signifies the attack loss $f(\boldsymbol{\delta}; \mathbf{x}_0, y_0, \mathcal{M}_i)$ given the natural input $(\mathbf{x}_0, y_0)$ and the model $\mathcal{M}_i$. Thus, problem (4) becomes

$$\operatorname*{minimize}_{\boldsymbol{\delta} \in \mathcal{X}} \operatorname*{maximize}_{\mathbf{w} \in \mathcal{P}} \quad \sum_{i=1}^{K} w_i f(\boldsymbol{\delta}; \mathbf{x}_0, y_0, \mathcal{M}_i) - \tfrac{\gamma}{2} \|\mathbf{w} - \mathbf{1}/K\|_2^2, \tag{5}$$

where $\mathbf{w}$ encodes the difficulty level of attacking each model.

Universal perturbation over multiple examples   Consider K natural examples $\{(\mathbf{x}_i, y_i)\}_{i=1}^{K}$ and a single model $\mathcal{M}$, our goal is to find the universal perturbation $\boldsymbol{\delta}$ so that all the corrupted K examples can fool $\mathcal{M}$. In this case, the notion of 'domain' in (4) is specified as 'example', and problem (4) becomes

$$\operatorname*{minimize}_{\boldsymbol{\delta} \in \mathcal{X}} \operatorname*{maximize}_{\mathbf{w} \in \mathcal{P}} \quad \sum_{i=1}^{K} w_i f(\boldsymbol{\delta}; \mathbf{x}_i, y_i, \mathcal{M}) - \tfrac{\gamma}{2} \|\mathbf{w} - \mathbf{1}/K\|_2^2, \tag{6}$$

where different from (5), $\mathbf{w}$ encodes the difficulty level of attacking each example.

Adversarial attack over data transformations Consider K categories of data transformation $\{p_i\}$, e.g., rotation, lightening, and translation (Athalye et al., 2018a), our goal is to find the adversarial attack that is robust to data transformations. In this case, the notion of 'domain' in (4) is specified as 'data transformer', and problem (4) becomes

$$\underset{\boldsymbol{\delta} \in \mathcal{X}}{\text{minimize}} \; \underset{\mathbf{w} \in \mathcal{P}}{\text{maximize}} \quad \sum_{i=1}^{K} w_i \mathbb{E}_{t \sim p_i}[f(t(\mathbf{x}_0 + \boldsymbol{\delta}); y_0, \mathcal{M})] - \frac{\gamma}{2} \|\mathbf{w} - \mathbf{1}/K\|_2^2, \tag{7}$$

where $\mathbb{E}_{t \sim p_i}[f(t(\mathbf{x}_0 + \boldsymbol{\delta}); y_0, \mathcal{M})]$ denotes the attack loss under the distribution of data transformation p_i, and $\mathbf{w}$ encodes the difficulty level of attacking each type of transformed example $\mathbf{x}_0$.

2.3 Adversarial training (AT) under mixed types of adversarial attacks

Conventional AT is restricted to a single type of norm-ball constrained adversarial attack (Madry et al., 2017). For example, AT under ℓ_∞ attack yields

$$\underset{\boldsymbol{\theta}}{\text{minimize}} \; \mathbb{E}_{(\mathbf{x},\mathbf{y}) \in \mathcal{D}} \; \underset{\|\boldsymbol{\delta}\|_\infty \leq \epsilon}{\text{maximize}} \; f_{\text{tr}}(\boldsymbol{\theta}, \boldsymbol{\delta}; \mathbf{x}, y), \tag{8}$$

where $\boldsymbol{\theta} \in \mathbb{R}^n$ denotes model parameters, $\boldsymbol{\delta}$ denotes ϵ-tolerant ℓ_∞ attack, and $f_{\text{tr}}(\boldsymbol{\theta}, \boldsymbol{\delta}; \mathbf{x}, y)$ is the training loss under perturbed examples $\{(\mathbf{x} + \boldsymbol{\delta}, y)\}$. However, there possibly exist blind attacking spots across multiple types of adversarial attacks so that AT under one attack would not be strong enough against another attack (Araujo et al., 2019). Thus, an interesting question is how to generalize AT under multiple types of adversarial attacks. One possible way is to use the finite-sum formulation

$$\underset{\boldsymbol{\theta}}{\text{minimize}} \; \mathbb{E}_{(\mathbf{x},\mathbf{y}) \in \mathcal{D}} \; \underset{\{\boldsymbol{\delta}_i \in \mathcal{X}_i\}}{\text{maximize}} \; \frac{1}{K} \sum_{i=1}^{K} f_{\text{tr}}(\boldsymbol{\theta}, \boldsymbol{\delta}_i; \mathbf{x}, y), \tag{9}$$

where $\boldsymbol{\delta}_i \in \mathcal{X}_i$ is the ith type of adversarial perturbation defined on $\mathcal{X}_i$, e.g., different ℓ_p attacks.

Moreover, one can map 'attack type' to 'domain' considered in (1). We then perform AT against the *strongest* adversarial attack across K attack types in order to avoid blind attacking spots. That is, upon defining $F_i(\boldsymbol{\theta}) := \text{maximize}_{\boldsymbol{\delta}_i \in \mathcal{X}_i} \; f_{\text{tr}}(\boldsymbol{\theta}, \boldsymbol{\delta}_i; \mathbf{x}, y)$, we solve the problem of the form (2),

$$\underset{\boldsymbol{\theta}}{\text{minimize}} \; \mathbb{E}_{(\mathbf{x},\mathbf{y}) \in \mathcal{D}} \; \underset{i \in [K]}{\text{maximize}} \; F_i(\boldsymbol{\theta}). \tag{10}$$

In fact, problem (10) is in the min-max-max form, however, Lemma 1 shows that problem (10) can be further simplified to the min-max form.

Lemma 1. *Problem* (10) *is equivalent to*

$$\underset{\boldsymbol{\theta}}{\text{minimize}} \; \mathbb{E}_{(\mathbf{x},\mathbf{y}) \in \mathcal{D}} \; \underset{\mathbf{w} \in \mathcal{P}, \{\boldsymbol{\delta}_i \in \mathcal{X}_i\}}{\text{maximize}} \; \sum_{i=1}^{K} w_i f_{\text{tr}}(\boldsymbol{\theta}, \boldsymbol{\delta}_i; \mathbf{x}, y), \tag{11}$$

where $\mathbf{w} \in \mathbb{R}^K$ *represent domain weights, and* $\mathcal{P}$ *has been defined in* (1).

Proof: see Appendix A.

Similar to (4), a strongly concave regularizer $-\gamma/2\|\mathbf{w} - \mathbf{1}/K\|_2^2$ can be added into the inner maximization problem of (11), which can boost the stability of the learning procedure and strike a balance between the max and the average attack performance. However, solving problem (11) and its regularized version is more complicated than (8) since the inner maximization involves both domain weights $\mathbf{w}$ and adversarial perturbations $\{\boldsymbol{\delta}_i\}$.

We finally remark that there was an *independent* work (Tramèr & Boneh, 2019) which also proposed the formulation (10) for AT under multiple perturbations. However, what we propose here is the regularized formulation of (11). As will be evident later, the domain weights $\mathbf{w}$ in our formulation have strong interpretability, which learns the importance level of different attacks. Most significantly, our work has different motivation from (Tramèr & Boneh, 2019), and our idea applies to not only AT but also attack generation in Sec. 2.2.

3 Proposed Algorithm and Theory

In this section, we delve into technical details on how to efficiently solve problems of robust adversarial attacks given by the generic form (4) and problem (11) for generalized AT under mixed types of adversarial attacks.

3.1 Alternating One-Step PGD for Robust Adversarial Attack Generation

We propose the **a**lternating one-step **p**rojected **g**radient **d**escent (APGD) method (Algorithm 1) to solve problem (4). For clarity, we repeat problem (4) under the adversarial perturbation $\boldsymbol{\delta}$ and its constraint set $\mathcal{X}$ defined in Sec. 2.2,

$$\operatorname*{minimize}_{\boldsymbol{\delta} \in \mathcal{X}} \operatorname*{maximize}_{\mathbf{w} \in \mathcal{P}} \quad \sum_{i=1}^{K} w_i F_i(\boldsymbol{\delta}). \qquad (12)$$

We show that at each iteration, APGD takes only one-step PGD for outer minimization and one-step projected gradient ascent for inner max-

---

Algorithm 1 APGD to solve problem (4)

1: Input: given $\mathbf{w}^{(0)}$ and $\boldsymbol{\delta}^{(0)}$.
2: **for** $t = 1, 2, \ldots, T$ **do**
3:     *outer min.*: fixing $\mathbf{w} = \mathbf{w}^{(t-1)}$, call PGD (13) to update $\boldsymbol{\delta}^{(t)}$
4:     *inner max.*: fixing $\boldsymbol{\delta} = \boldsymbol{\delta}^{(t)}$, update $\mathbf{w}^{(t)}$ via (14)
5: **end for**

---

imization (namely, PGD for its negative objective function). We also show that each alternating step has a closed-form expression, and the main computational complexity stems from computing the gradient of the attack loss w.r.t. the input. Therefore, APGD is computationally efficient like PGD, which is commonly used for design of conventional single ℓ_p-norm based adversarial attacks (Madry et al., 2017).

Outer minimization   Considering $\mathbf{w} = \mathbf{w}^{(t-1)}$ and $F(\boldsymbol{\delta}) := \sum_{i=1}^{K} w_i^{(t-1)} F_i(\boldsymbol{\delta})$ in (4), we perform one-step PGD to update $\boldsymbol{\delta}$ at iteration t,

$$\boldsymbol{\delta}^{(t)} = \operatorname{proj}_{\mathcal{X}} \left(\boldsymbol{\delta}^{(t-1)} - \alpha \nabla_{\boldsymbol{\delta}} F(\boldsymbol{\delta}^{(t-1)}) \right), \qquad (13)$$

where $\operatorname{proj}(\cdot)$ denotes the Euclidean projection operator, i.e., $\operatorname{proj}_{\mathcal{X}}(\mathbf{a}) = \arg\min_{\mathbf{x} \in \mathcal{X}} \|\mathbf{x} - \mathbf{a}\|_2^2$ at the point $\mathbf{a}$, $\alpha > 0$ is a given learning rate, and $\nabla_{\boldsymbol{\delta}}$ denotes the first order gradient w.r.t. $\boldsymbol{\delta}$.

In (13), the projection operation becomes the key to obtain the closed-form of the updating rule (13). Recall from Sec. 2.2 that $\mathcal{X} = \{\boldsymbol{\delta} | \|\boldsymbol{\delta}\|_p \leq \epsilon, \check{\mathbf{c}} \leq \boldsymbol{\delta} \leq \hat{\mathbf{c}}\}$, where $p \in \{0, 1, 2, \infty\}$, and $\check{\mathbf{c}} = -\mathbf{x}_0$ and $\hat{\mathbf{c}} = \mathbf{1} - \mathbf{x}_0$ (implying $\check{\mathbf{c}} \leq \mathbf{0} \leq \hat{\mathbf{c}}$). If $p = \infty$, then the projection function becomes the clip function. However, when $p \in \{0, 1, 2\}$, the closed-form of projection operation becomes non-trivial. In Proposition 1, we derive the solution of $\operatorname{proj}_{\mathcal{X}}(\mathbf{a})$ under different ℓ_p norms.

Proposition 1. *Given a point $\mathbf{a} \in \mathbb{R}^d$ and a constraint set $\mathcal{X} = \{\boldsymbol{\delta} | \|\boldsymbol{\delta}\|_p \leq \epsilon, \check{\mathbf{c}} \leq \boldsymbol{\delta} \leq \hat{\mathbf{c}}\}$, the Euclidean projection $\boldsymbol{\delta}^* = \operatorname{proj}_{\mathcal{X}}(\mathbf{a})$ has a closed-form solution when $p \in \{0, 1, 2\}$.*

Proof: See Appendix B. $\qquad\qquad\qquad\qquad\qquad\qquad\qquad\qquad\qquad\qquad\qquad\qquad\square$

Inner maximization   By fixing $\boldsymbol{\delta} = \boldsymbol{\delta}^{(t)}$ and letting $\psi(\mathbf{w}) := \sum_{i=1}^{K} w_i F_i(\boldsymbol{\delta}^{(t)}) - \frac{\gamma}{2} \|\mathbf{w} - \mathbf{1}/K\|_2^2$ in problem (4), we then perform one-step PGD (w.r.t. $-\psi$) to update $\mathbf{w}$,

$$\mathbf{w}^{(t)} = \operatorname{proj}_{\mathcal{P}} \Big(\underbrace{\mathbf{w}^{(t-1)} + \beta \nabla_{\mathbf{w}} \psi(\mathbf{w}^{(t-1)})}_{\mathbf{b}} \Big) = (\mathbf{b} - \mu\mathbf{1})_+, \qquad (14)$$

where $\beta > 0$ is a given learning rate, $\nabla_{\mathbf{w}} \psi(\mathbf{w}) = \boldsymbol{\phi}^{(t)} - \gamma(\mathbf{w} - \mathbf{1}/K)$, and $\boldsymbol{\phi}^{(t)} := [F_1(\boldsymbol{\delta}^{(t)}), \ldots, F_K(\boldsymbol{\delta}^{(t)})]^T$. In (14), the second equality holds due to the closed-form of projection operation onto the probabilistic simplex $\mathcal{P}$ (Parikh et al., 2014), where $(\cdot)_+$ denotes the elementwise nonnegative operator, i.e., $(x)_+ = \max\{0, x\}$, and μ is the root of the equation $\mathbf{1}^T(\mathbf{b} - \mu\mathbf{1})_+ = 1$. Since $\mathbf{1}^T(\mathbf{b} - \min_i\{b_i\}\mathbf{1} + \mathbf{1}/K)_+ \geq \mathbf{1}^T\mathbf{1}/K = 1$, and $\mathbf{1}^T(\mathbf{b} - \max_i\{b_i\}\mathbf{1} + \mathbf{1}/K)_+ \leq \mathbf{1}^T\mathbf{1}/K = 1$, the root μ exists within the interval $[\min_i\{b_i\} - 1/K, \max_i\{b_i\} - 1/K]$ and can be found via the bisection method (Boyd & Vandenberghe, 2004).

Convergence analysis   We remark that APGD follows the gradient primal-dual optimization framework (Lu et al., 2019a), and thus enjoys the same optimization guarantees. In Theorem 1, we demonstrate the convergence rate of Algorithm 1 for solving problem (4).

Theorem 1. *(inherited from primal-dual min-max optimization) Suppose that in problem (4) $F_i(\boldsymbol{\delta})$ has L-Lipschitz continuous gradients, and $\mathcal{X}$ is a convex compact set. Given learning rates $\alpha \leq \frac{1}{L}$ and $\beta < \frac{1}{\gamma}$, then the sequence $\{\boldsymbol{\delta}^{(t)}, \mathbf{w}^{(t)}\}_{t=1}^{T}$ generated by Algorithm 1 converges to a first-order stationary point[2] of problem (4) under the convergence rate $O(\frac{1}{T})$.*

---

[2]The stationarity is measured by the ℓ_2 norm of gradient of the objective in (4) w.r.t. $(\boldsymbol{\delta}, \mathbf{w})$.

Proof: Note that the objective function of problem (4) is strongly concave w.r.t. $\mathbf{w}$ with parameter γ, and has γ-Lipschitz continuous gradients. Moreover, we have $\|\mathbf{w}\|_2 \leq 1$ due to $\mathbf{w} \in \mathcal{P}$. Using these facts and (Lu et al., 2019a, Theorem 1) or (Lu et al., 2019b, Theorem 1) completes the proof. □

3.2 ALTERNATING MULTI-STEP PGD FOR GENERALIZED AT

We next propose the **a**lternating **m**ulti-step **p**rojected **g**radient **d**escent (AMPGD) method to solve the regularized version of problem (11), which is repeated as follows

$$\underset{\boldsymbol{\theta}}{\text{minimize}} \; \mathbb{E}_{(\mathbf{x},\mathbf{y})\in\mathcal{D}} \; \underset{\mathbf{w}\in\mathcal{P},\{\boldsymbol{\delta}_i\in\mathcal{X}_i\}}{\text{maximize}} \; \psi(\boldsymbol{\theta},\mathbf{w},\{\boldsymbol{\delta}_i\}) := \sum_{i=1}^{K} w_i f_{\text{tr}}(\boldsymbol{\theta},\boldsymbol{\delta}_i;\mathbf{x},y) - \frac{\gamma}{2}\|\mathbf{w} - \mathbf{1}/K\|_2^2. \tag{15}$$

Problem (15) is in a more general non-convex non-concave min-max setting, where the inner maximization involves both domain weights $\mathbf{w}$ and adversarial perturbations $\{\boldsymbol{\delta}_i\}$. It was shown in (Nouiehed et al., 2019) that the multi-step PGD is required for inner maximization in order to approximate the near-optimal solution. This is also in the similar spirit of AT (Madry et al., 2017), which executed multi-step PGD attack during inner maximization. We summarize AMPGD in Algorithm 2. At step 4 of Algorithm 2, each PGD step to update $\mathbf{w}$ and $\boldsymbol{\delta}$ can be decomposed as

---

Algorithm 2 AMPGD to solve problem (15)

1: **Input:** given $\boldsymbol{\theta}^{(0)}$, $\mathbf{w}^{(0)}$, $\boldsymbol{\delta}^{(0)}$ and $K > 0$.
2: **for** $t = 1, 2, \ldots, T$ **do**
3:    given $\mathbf{w}^{(t-1)}$ and $\boldsymbol{\delta}^{(t-1)}$, perform SGD to update $\boldsymbol{\theta}^{(t)}$ (Madry et al., 2017)
4:    given $\boldsymbol{\theta}^{(t)}$, perform R-step PGD to update $\mathbf{w}^{(t)}$ and $\boldsymbol{\delta}^{(t)}$
5: **end for**

$$\mathbf{w}_r^{(t)} = \text{proj}_{\mathcal{P}}\left(\mathbf{w}_{r-1}^{(t)} + \beta\nabla_{\mathbf{w}}\psi(\boldsymbol{\theta}^{(t)},\mathbf{w}_{r-1}^{(t)},\{\boldsymbol{\delta}_{i,r-1}^{(t)}\})\right), \forall r \in [R],$$

$$\boldsymbol{\delta}_{i,r}^{(t)} = \text{proj}_{\mathcal{X}_i}\left(\boldsymbol{\delta}_{i,r-1}^{(t)} + \beta\nabla_{\boldsymbol{\delta}}\psi(\boldsymbol{\theta}^{(t)},\mathbf{w}_{r-1}^{(t)},\{\boldsymbol{\delta}_{i,r-1}^{(t)}\})\right), \forall r \in [R], \forall i \in [K]$$

where let $\mathbf{w}_1^{(t)} := \mathbf{w}^{(t-1)}$ and $\boldsymbol{\delta}_{i,1}^{(t)} := \boldsymbol{\delta}_i^{(t-1)}$. Here the subscript t represents the iteration index of AMPGD, and the subscript r denotes the iteration index of R-step PGD. Clearly, the above projection operations can be derived for closed-form expressions through (14) and Lemma 1. To the best of our knowledge, it is still an open question to build theoretical convergence guarantees for solving the general non-convex non-concave min-max problem like (15), except the work (Nouiehed et al., 2019) which proposed $O(1/T)$ convergence rate if the objective function satisfies Polyak-Łojasiewicz conditions (Karimi et al., 2016).

Improved robustness via diversified ℓ_p attacks.   It was recently shown in (Kariyappa & Qureshi, 2019; Pang et al., 2019) that the diversity of individual neural networks improves adversarial robustness of an ensemble model. Spurred by that, one may wonder if the promotion of diversity among ℓ_p attacks is beneficial to adversarial robustness? We measure the diversity between adversarial attacks through the similarity between perturbation directions, namely, input gradients $\{\nabla_{\boldsymbol{\delta}_i} f_{\text{tr}}(\boldsymbol{\theta},\boldsymbol{\delta}_i;\mathbf{x},y)\}_i$ in (15). We find that there exists a strong correlation between input gradients for different ℓ_p attacks. Thus, we propose to enhance their diversity through the orthogonality-promoting regularizer used for encouraging diversified prediction of ensemble models in (Pang et al., 2019),

$$h(\boldsymbol{\theta},\{\boldsymbol{\delta}_i\};\mathbf{x},y) := \log\det(\mathbf{G}^T\mathbf{G}), \tag{16}$$

where $\mathbf{G} \in \mathbb{R}^{d\times K}$ is a $d \times K$ matrix, each column of which corresponds to a normalized input gradient $\nabla_{\boldsymbol{\delta}_i} f_{\text{tr}}(\boldsymbol{\theta},\boldsymbol{\delta}_i;\mathbf{x},y)$ for $i \in [K]$, and $h(\boldsymbol{\theta},\{\boldsymbol{\delta}_i\};\mathbf{x},y)$ reaches the maximum value 0 as input gradients become orthogonal. With the aid of (16), we modify problem (15) to

$$\underset{\boldsymbol{\theta}}{\text{minimize}} \; \mathbb{E}_{(\mathbf{x},\mathbf{y})\in\mathcal{D}} \; \underset{\mathbf{w}\in\mathcal{P},\{\boldsymbol{\delta}_i\in\mathcal{X}_i\}}{\text{maximize}} \; \psi(\boldsymbol{\theta},\mathbf{w},\{\boldsymbol{\delta}_i\}) + \lambda h(\boldsymbol{\theta},\{\boldsymbol{\delta}_i\};\mathbf{x},y). \tag{17}$$

The rationale behind (17) is that the adversary aims to enhance the effectiveness of attacks from diversified perturbation directions (inner maximization), while the defender robustifies the model $\boldsymbol{\theta}$, which makes diversified attacks less effective (outer minimization).

4 EXPERIMENTS

In this section, we first evaluate the proposed min-max optimization strategy on three attack tasks. We show that our approach leads to substantial improvement compared with state-of-the-art attack

Table 1: Comparison of average and min-max (APGD) ensemble attack over four models on MNIST and CIFAR-10. Acc (%) represents the test accuracy of classifiers on adversarial examples. Here we set the iterations of APGD as 50 for attack generation. The learning rates α, β and regularization factor γ are provided in Appendix C.2.

(a) MNIST

Box constraint	Opt.	Acc_A	Acc_B	Acc_C	Acc_D	ASR_{all}	Lift ($\uparrow$)
ℓ_0 ($\epsilon = 30$)	avg.	7.03	1.51	11.27	2.48	84.03	-
	min max	3.65	2.36	4.99	3.11	**91.97**	**9.45%**
ℓ_1 ($\epsilon = 20$)	avg.	20.79	0.15	21.48	6.70	69.31	-
	min max	6.12	2.53	8.43	5.11	**89.16**	**28.64%**
ℓ_2 ($\epsilon = 3.0$)	avg.	6.88	0.03	26.28	14.50	69.12	-
	min max	1.51	0.89	3.50	2.06	**95.31**	**37.89%**
ℓ_∞ ($\epsilon = 0.2$)	avg.	1.05	0.07	41.10	35.03	48.17	-
	min max	2.47	0.37	7.39	5.81	**90.16**	**87.17%**

(b) CIFAR-10

Box constraint	Opt.	Acc_A	Acc_B	Acc_C	Acc_D	ASR_{all}	Lift ($\uparrow$)
ℓ_0 ($\epsilon = 50$)	avg.	27.86	3.15	5.16	6.17	65.16	-
	min max	18.74	8.66	9.64	9.70	**71.44**	**9.64%**
ℓ_1 ($\epsilon = 30$)	avg.	32.92	2.07	5.55	6.36	59.74	-
	min max	12.46	3.74	5.62	5.86	**78.65**	**31.65%**
ℓ_2 ($\epsilon = 2.0$)	avg.	24.3	1.51	4.59	4.20	69.55	-
	min max	7.17	3.03	4.65	5.14	**83.95**	**20.70%**
ℓ_∞ ($\epsilon = 0.05$)	avg.	19.69	1.55	5.61	4.26	73.29	-
	min max	7.21	2.68	4.74	4.59	**84.36**	**15.10%**

methods such as ensemble PGD (Liu et al., 2018) and expectation over transformation (EOT) (Athalye et al., 2018b; Brown et al., 2017; Athalye et al., 2018a). We next demonstrate the effectiveness of the generalized AT for multiple types of adversarial perturbations. We show that the use of trainable domain weights in problem (15) can automatically adjust the risk level of different attacks during the training process even if the defender lacks prior knowledge on the strength of these attacks. We also show that the promotion of diversity of ℓ_p attacks help improve adversarial robustness further.

We thoroughly evaluate our APGD/AMPGD algorithm on MNIST and CIFAR-10. A set of diverse image classifiers (denoted from Model A to Model H) are trained, including multi-layer perceptrons (MLP), All-CNNs (Springenberg et al., 2015), LeNet (Lecun et al., 1998), LeNetV2, VGG16 (Simonyan & Zisserman, 2015), ResNet50 (He et al., 2016), Wide-ResNet (Madry et al., 2017; Zagoruyko & Komodakis, 2016) and GoogLeNet (Szegedy et al., 2015). More details about model architectures and training process are provided in Appendix C.1.

4.1 ROBUST ADVERSARIAL ATTACKS

Most current works play a min-max game from a defender's perspective, i.e., adversarial training. However, we show the great strength of min-max optimization also lies at the side of attack generation. Note that problem formulations (5)-(7) are applicable to both *untargeted* and *targeted* attack. Here we focus on the former setting and use C&W loss function (Carlini & Wagner, 2017; Madry et al., 2017). The details of crafting adversarial examples are available in Appendix C.2.

Ensemble attack over multiple models We craft adversarial examples against an ensemble of known classifiers. The work (Liu et al., 2018, 5th place at CAAD-18) proposed an ensemble PGD attack, which assumed equal importance among different models, namely, $w_i = 1/K$ in problem (1). Throughout this task, we measure the attack performance via **ASR_{all}** - the attack success rate (ASR) of fooling model ensembles simultaneously. Compared to the ensemble PGD attack (Liu et al., 2018), **our approach results in 40.79% and 17.48% ASR_{all} improvement averaged over different ℓ_p-norm constraints on MNIST and CIFAR-10**, respectively. In what follows, we provide more detailed experiment results and analysis.

In Table 1, we show that our min-max APGD significantly outperforms ensemble PGD in ASR_{all}. Taking ℓ_∞-attack on MNIST as an example, our min-max attack leads to a 90.16% ASR_{all}, which largely outperforms 48.17% (ensemble PGD). The reason is that Model C, D are more difficult to attack, which can be observed from their higher test accuracy on adversarial examples. As a result, although the adversarial examples crafted by assigning equal weights over multiple models are able to attack {A, B} well, they achieve a much lower ASR (i.e., 1 - Acc) in {C, D}. By contrast, APGD automatically handles the worst case {C, D} by slightly sacrificing the performance on {A, B}: 31.47% averaged ASR improvement on {C, D} versus 0.86% degradation on {A, B}. More results on CIFAR-10 and more complicated DNNs (e.g., GoogLeNet) are provided in Appendix D.

Figure 1 depicts the ASR of four models under average/min-max attacks as well as the distribution of domain weights during attack generation. For ensemble PGD (Figure 1a), Model C and D are attacked insufficiently, leading to relatively low ASR and thus weak ensemble performance. By contrast, APGD (Figure 1b) will encode the difficulty level to attack different models based on the current attack loss. It dynamically adjusts the weight w_i as shown in Figure 1c. For instance, the weight for Model D is first raised to 0.45 because D is difficult to attack initially. Then it decreases to

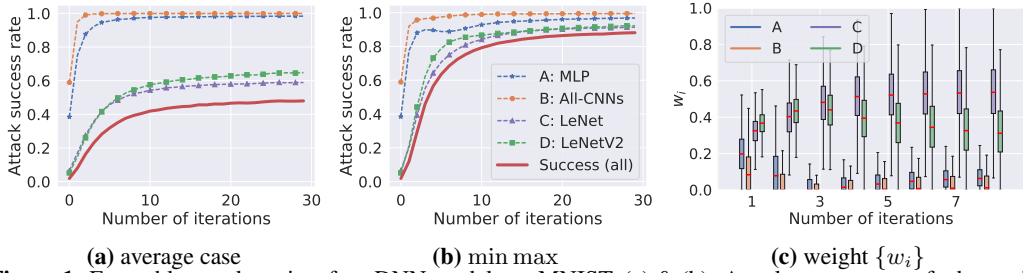**(a)** average case   **(b)** min max   **(c)** weight $\{w_i\}$

Figure 1: Ensemble attack against four DNN models on MNIST. (a) & (b): Attack success rate of adversarial examples generated by average (ensemble PGD) or min-max (APGD) attack method. (c): Boxplot of weight w in APGD adversarial loss for four models. Here we adopt the same ℓ_∞-attack as Table 1.
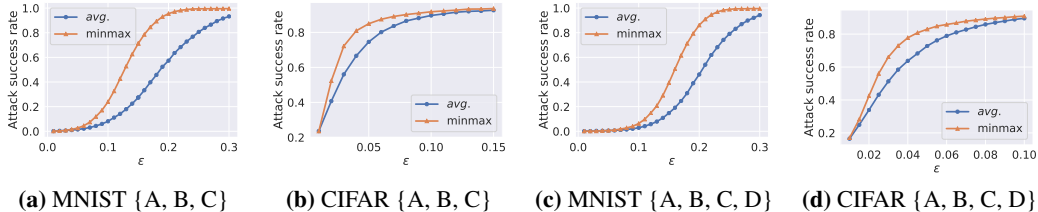

(a) MNIST {A, B, C}   **(b)** CIFAR {A, B, C}   **(c)** MNIST {A, B, C, D}   **(d)** CIFAR {A, B, C, D}

Figure 2: ASR of average and min-max ℓ_∞ ensemble attack versus maximum perturbation magnitude ϵ.

0.3 once Model D encounters the sufficient attack power and the corresponding attack performance is no longer improved. It is worth noticing that APGD is highly efficient because w_i converges after a small number of iterations. To perform a boarder evaluation, we repeat the above experiments (ℓ_∞ norm) under different ϵ in Figure 2. The ASR of min-max strategy is consistently better or on part with the average strategy. Moreover, APGD achieves more significant improvement when moderate ϵ is chosen: MNIST ($\epsilon \in [0.15, 0.25]$) and CIFAR-10 ($\epsilon \in [0.03, 0.05]$).

Lastly, we highlight that tracking domain weights **w** provides us novel insights for model robustness and understanding attack procedure. From our theory, a model with higher robustness always corresponds to a larger w because its loss is hard to attack and becomes the "worst" term. This hypothesis can be verified empirically. According to Figure 1c, we have $w_c > w_d > w_a > w_b$ – indicating a decrease in model robustness for C, D, A and B, which is exactly verified by $\text{Acc}_C > \text{Acc}_D > \text{Acc}_A > \text{Acc}_B$ in Table 1 (ℓ_∞-norm).

Universal perturbation over multiple examples We evaluate APGD in universal perturbation on MNIST and CIFAR-10, where 10,000 test images are randomly divided into equal-size groups (containing K images per group) for universal perturbation. We measure two types of ASR (%), **ASR**$_{avg}$ and **ASR**$_{gp}$. Here the former represents the ASR averaged over all images in all groups, and the latter signifies the ASR averaged over all groups but a successful attack is counted under a more restricted condition: images within each group must be successfully attacked simultaneously by universal perturbation. **When $K = 5$, our approach achieves 42.63% and 35.21% improvement over the averaging strategy under MNIST and CIFAR-10, respectively.**

In Table 2, we compare the proposed min-max strategy (APGD) with the averaging strategy on the attack performance of generated universal perturbations. As we can see, our method always achieves higher ASR$_{gp}$ for different values of K. The universal perturbation generated from APGD can successfully attack 'hard' images (on which the average-based PGD attack fails) by self-adjusting domain weights, and thus leads to a higher ASR$_{gp}$. Besides, the min-max universal perturbation also offers interpretability of "image robustness" by associating domain weights with image visualization; see Figure A9 and A10 (Appendix F) for an example in which the large domain weight corresponds to the MNIST letter with clear appearance (e.g., bold letter).

Robust adversarial attack over data transformations EOT (Athalye et al., 2018a) achieves state-of-the-art performance in producing adversarial examples robust to data transformations. From (7), we could derive EOT as a special case when the weights satisfy $w_i = 1/K$ (average case). For each input sample (*ori*), we transform the image under a series of functions, e.g., flipping horizontally

Table 2: Comparison of average and minmax optimization on universal perturbation over multiple input examples. The adversarial examples are generated by 20-step ℓ_∞-APGD with $\alpha = \frac{1}{6}, \beta = \frac{1}{50}$ and $\gamma = 4$.

Setting			$K=2$			$K=4$			$K=5$			$K=10$		
Dataset	Model	Opt.	ASR_{avg}	ASR_{gp}	Lift (↑)	ASR_{avg}	ASR_{gp}	Lift (↑)	ASR_{avg}	ASR_{gp}	Lift (↑)	ASR_{avg}	ASR_{gp}	Lift (↑)
MNIST	MLP	avg.	97.19	94.48	-	85.13	56.64	-	79.11	38.05	-	60.53	3.50	-
		min max	98.15	**96.96**	**2.62%**	83.76	**72.32**	**27.68%**	72.28	**53.70**	**41.13%**	30.10	**6.70**	**91.43%**
	All-CNNs	avg.	97.76	95.52	-	85.19	51.92	-	80.02	31.25	-	65.79	2.10	-
		min max	99.69	**99.38**	**4.04%**	90.11	**75.64**	**45.69%**	80.21	**53.50**	**71.20%**	43.54	**4.30**	**104.8%**
	LeNet	avg.	94.78	89.96	-	62.12	28.72	-	51.84	19.15	-	30.29	4.30	-
		min max	96.60	**94.58**	**5.14%**	55.50	**36.72**	**27.86%**	42.79	**25.80**	**34.73%**	22.48	**7.20**	**67.44%**
	LeNetV2	avg.	94.72	90.04	-	61.59	26.60	-	50.42	17.05	-	26.49	4.80	-
		min max	97.33	**95.68**	**6.26%**	55.38	**35.52**	**33.53%**	40.22	**21.05**	**23.46%**	19.73	**7.10**	**47.92%**
CIFAR-10	All-CNNs	avg.	91.09	83.08	-	85.66	54.72	-	82.76	40.20	-	71.22	4.50	-
		min max	92.22	**85.98**	**3.49%**	87.63	**65.80**	**20.25%**	85.02	**55.74**	**38.66%**	65.64	**11.80**	**162.2%**
	LeNetV2	avg.	93.26	86.90	-	90.04	66.12	-	88.28	55.00	-	72.02	8.90	-
		min max	93.34	**87.08**	**0.21%**	91.91	**71.64**	**8.35%**	91	**63.55**	**15.55%**	82.85	**25.10**	**182.0%**
	VGG16	avg.	90.76	82.56	-	89.36	63.92	-	88.74	55.20	-	85.86	22.40	-
		min max	92.40	**85.92**	**4.07%**	90.04	**70.40**	**10.14%**	88.97	**63.30**	**14.67%**	79.07	**30.80**	**37.50%**
	GoogLeNet	avg.	85.02	72.48	-	75.20	32.68	-	71.82	19.60	-	59.01	0.40	-
		min max	87.08	**77.82**	**7.37%**	77.05	**46.20**	**41.37%**	71.20	**33.70**	**71.94%**	45.46	**2.40**	**600.0%**

Table 3: Comparison of average and min-max optimization on robust attack over multiple data transformations on CIFAR-10. Acc (%) represents the test accuracy of classifiers on adversarial examples (20-step ℓ_∞-APGD ($\epsilon = 0.03$) with $\alpha = \frac{1}{2}, \beta = \frac{1}{100}$ and $\gamma = 10$) under different transformations.

Model	Opt.	Acc_{ori}	Acc_{flh}	Acc_{flv}	Acc_{bri}	Acc_{gam}	Acc_{crop}	ASR_{avg}	ASR_{gp}	Lift (↑)
A	avg.	10.80	21.93	14.75	11.52	10.66	20.03	85.05	55.88	-
	min max	12.14	18.05	13.61	13.52	11.99	16.78	85.65	**60.03**	**7.43%**
B	avg.	5.49	11.56	9.51	5.43	5.75	15.89	91.06	72.21	-
	min max	6.22	8.61	9.74	6.35	6.42	11.99	91.78	**77.43**	**7.23%**
C	avg.	7.66	21.88	15.50	8.15	7.87	15.36	87.26	56.51	-
	min max	8.51	14.75	13.88	9.16	8.58	13.35	88.63	**63.58**	**12.51%**
D	avg.	8.00	20.47	13.46	7.73	8.52	15.90	87.65	61.13	-
	min max	9.19	13.18	12.72	8.79	9.18	13.11	88.97	**67.49**	**10.40%**

(*flh*) or vertically (*flv*), adjusting brightness (*bri*), performing gamma correction (*gam*) and cropping (*crop*), and group each image with its transformed variants. Similar to universal perturbation, ASR_{avg} and ASR_{gp} are reported to measure the ASR over all transformed images and groups of transformed images (each group is successfully attacked signifies successfully attacking an example under all transformers). In Table 3, **compared to EOT, our approach leads to 9.39% averaged lift in ASR_{gp}** over given models on CIFAR-10 by optimizing the weights for various transformations. Due to limited space, we leave the details of transformers in Append C.3 and the results under randomness (e.g., flipping images randomly *w.p.* 0.8; randomly clipping the images at specific range) in Appendix D.

4.2 ADVERSARIAL TRAINING FOR MULTIPLE ADVERSARIAL PERTURBATIONS

Compared to vanilla AT, we show the generalized AT scheme produces models robust to multiple types of perturbation, thus leads to stronger "overall robustness". We measure the training performance using two types of Acc (%): $\textbf{Acc}_{adv}^{max}$ and $\textbf{Acc}_{adv}^{avg}$, where Acc_{adv}^{max} denotes the test accuracy over examples with the strongest perturbation (ℓ_∞ or ℓ_2), and Acc_{adv}^{avg} denotes the averaged test accuracy over examples with all types of perturbations (ℓ_∞ and ℓ_2). Moreover, we measure the **overall worst-case robustness** S_ϵ in terms of the area under the curve 'Acc_{adv}^{max} vs. ϵ' (see Figure 3b).

In Table 4, we present the test accuracy of MLP in different training schemes: a) natural training, b) single-norm: vanilla AT (ℓ_∞ or ℓ_2), c) multi-norm: generalized AT (*avg* and min max), and d) generalized AT with diversity-promoting attack regularization (DPAR, $\lambda = 0.1$ in problem (16)). If the adversary only performs single-type attack, training and testing on the same attack type leads to the best performance (diagonal of ℓ_∞-ℓ_2 block). However, when facing ℓ_∞ and ℓ_2 attacks simultaneously, multi-norm generalized AT achieves better Acc_{adv}^{max} and Acc_{adv}^{avg} than single-norm AT. In particular, the min-max strategy slightly outperforms the averaging strategy under multiple perturbation norms.

Table 4: Adversarial training of MNIST models on single attacks (ℓ_∞ and ℓ_2) and multiple attacks ($avg.$ and min max). The perturbation magnitude ϵ for ℓ_∞ and ℓ_2 attacks are 0.2 and 2.0, respectively. Top 2 test accuracy on each metric are highlighted. Complete table for varied ϵ is given in Table A8 (Appendix E).

(a) MLP

Opt.	Acc.	Acc-ℓ_∞	Acc-ℓ_2	$\text{Acc}_{\text{adv}}^{\text{max}}$	$\text{Acc}_{\text{adv}}^{\text{avg}}$
natural	98.30	2.70	13.86	0.85	8.28
ℓ_∞	98.08	**77.70**	69.17	66.34	73.43
ℓ_2	98.72	70.03	**81.74**	69.14	75.88
$avg.$	98.62	75.09	79.00	72.23	77.05
+ DPAR	98.50	76.75	79.67	**74.14**	**78.21**
min max	98.59	75.96	79.15	73.43	77.55
+ DPAR	98.58	**76.92**	**79.74**	**74.29**	**78.35**

(b) LeNet

Opt.	Acc.	Acc-ℓ_∞	Acc-ℓ_2	$\text{Acc}_{\text{adv}}^{\text{max}}$	$\text{Acc}_{\text{adv}}^{\text{avg}}$
natural	99.25	17.93	39.32	17.57	28.63
ℓ_∞	99.18	**93.80**	78.97	78.80	86.39
ℓ_2	99.22	85.84	**87.31**	84.06	86.58
$avg.$	99.22	88.96	85.59	84.29	87.28
+ DPAR	99.25	89.96	**86.49**	**85.44**	**88.23**
min max	99.32	89.21	85.98	84.82	87.60
+ DPAR	99.22	**90.19**	86.47	**85.47**	**88.33**

(a) weight $\{w_i\}$ **(b)** $\text{Acc}_{\text{adv}}^{\text{max}}$ **(c)** $\text{Acc}_{\text{adv}}^{\text{avg}}$
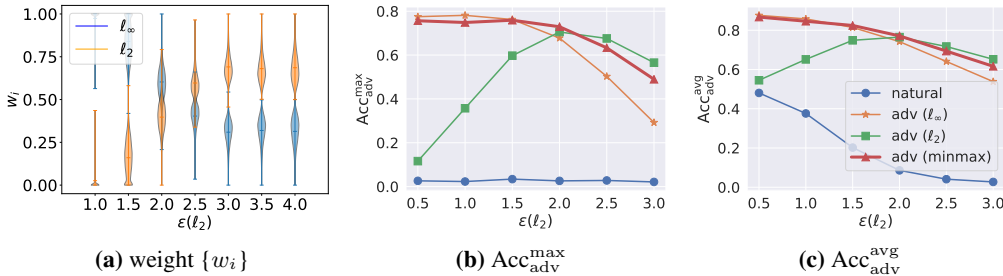
Figure 3: (a): Violin plot of weight w in APGD versus perturbation magnitude ϵ of ℓ_2-attack in AT; (b) & (c): Robustness of MLP under different AT schemes. Supplementary result for LeNet is provided in Figure A2 (Appendix E).

DPAR further boosts the adversarial test accuracy, which implies that the promotion of diversified ℓ_p attacks is a beneficial supplement to adversarial training.

In Figure 3, we offer deeper insights on the performance of generalized AT. During the training procedure we fix ϵ_{ℓ_∞} (ϵ for ℓ_∞ attack during training) as 0.2, and change ϵ_{ℓ_2} from 0.2 to 5.6 ($\epsilon_{\ell_\infty} \times \sqrt{d}$) so that the ℓ_∞ and ℓ_2 balls are not completely overlapped (Araujo et al., 2019). In Figure 3a, as ϵ_{ℓ_2} increases, ℓ_2-attack becomes stronger so the corresponding w also increases, which is consistent with min-max spirit – defending the strongest attack. We remark that min max or avg training does not always lead to the best performance on $\text{Acc}_{\text{adv}}^{\text{max}}$ and $\text{Acc}_{\text{adv}}^{\text{avg}}$, especially when the strengths of two attacks diverge greatly (see Table A8). This can be explained by the large overlapping between ℓ_∞ and ℓ_2 balls (see Figure A3). However, Figure 3b and 3c show that AMPGD is able to achieve a rather robust model no matter how ϵ changes (red lines), which empirically verifies the effectiveness of our proposed training scheme. In terms of the area-under-the-curve measure S_ϵ, **AMPGD achieves the highest worst-case robustness: 6.27% and 17.64% improvement compared to the vanilla AT with ℓ_∞ and ℓ_2 attacks**. Furthermore, we show in Figure A4a that our min-max scheme leads to faster convergence than the averaging scheme due to the benefit of self-adjusted domain weights.

5 Conclusion

In this paper, we propose a general min-max framework applicable to both adversarial attack and defense settings. We show that many problem setups can be re-formulated under this general framework. Extensive experiments show that proposed algorithms lead to significant improvement on multiple attack and defense tasks compared with previous state-of-the-art approaches. In particular, we obtain 17.48%, 35.21% and 9.39% improvement on attacking model ensembles, devising universal perturbation to input samples, and data transformations under CIFAR-10, respectively. Our min-max scheme also generalizes adversarial training (AT) for multiple types of adversarial attacks, attaining faster convergence and better robustness compared to the vanilla AT and the average strategy. Moreover, our approach provides a holistic tool for self-risk assessment by learning domain weights.

REFERENCES

Alexandre Araujo, Rafael Pinot, Benjamin Negrevergne, Laurent Meunier, Yann Chevaleyre, Florian Yger, and Jamal Atif. Robust neural networks using randomized adversarial training. *arXiv preprint arXiv:1903.10219*, 2019.

A. Athalye, L. Engstrom, A. Ilyas, and K. Kwok. Synthesizing robust adversarial examples. In Jennifer Dy and Andreas Krause (eds.), *Proceedings of the 35th International Conference on Machine Learning*, volume 80, pp. 284–293, 10–15 Jul 2018a.

Anish Athalye and Ilya Sutskever. Synthesizing robust adversarial examples. *ICML*, 2018.

Anish Athalye, Nicholas Carlini, and David Wagner. Obfuscated gradients give a false sense of security: Circumventing defenses to adversarial examples. *arXiv preprint arXiv:1802.00420*, 2018b.

S. Boyd and L. Vandenberghe. *Convex optimization*. Cambridge university press, 2004.

Tom B. Brown, Dandelion Mané, Aurko Roy, Martín Abadi, and Justin Gilmer. Adversarial patch. *CoRR*, abs/1712.09665, 2017.

Nicholas Carlini and David Wagner. Towards evaluating the robustness of neural networks. In *Security and Privacy (SP), 2017 IEEE Symposium on*, pp. 39–57. IEEE, 2017.

Nicholas Carlini and David A. Wagner. Audio adversarial examples: Targeted attacks on speech-to-text. In *IEEE Symposium on Security and Privacy Workshops*, pp. 1–7. IEEE Computer Society, 2018.

Nicholas Carlini, Pratyush Mishra, Tavish Vaidya, Yuankai Zhang, Micah Sherr, Clay Shields, David Wagner, and Wenchao Zhou. Hidden voice commands. In *USENIX Security Symposium*, pp. 513–530, 2016.

Nicholas Carlini, Anish Athalye, Nicolas Papernot, Wieland Brendel, Jonas Rauber, Dimitris Tsipras, Ian J. Goodfellow, Aleksander Madry, and Alexey Kurakin. On evaluating adversarial robustness. *CoRR*, abs/1902.06705, 2019.

Hongge Chen, Huan Zhang, Pin-Yu Chen, Jinfeng Yi, and Cho-Jui Hsieh. Attacking visual language grounding with adversarial examples: A case study on neural image captioning. In *Proceedings of the 56th Annual Meeting of the Association for Computational Linguistics*, volume 1, pp. 2587–2597, 2018a.

Pin-Yu Chen, Yash Sharma, Huan Zhang, Jinfeng Yi, and Cho-Jui Hsieh. EAD: elastic-net attacks to deep neural networks via adversarial examples. *AAAI*, 2018b.

Francesco Croce and Matthias Hein. Provable robustness against all adversarial l_p-perturbations for $p \geq 1$. *arXiv preprint arXiv:1905.11213*, 2019.

K. Eykholt, I. Evtimov, E. Fernandes, B. Li, A. Rahmati, C. Xiao, A. Prakash, T. Kohno, and D. Song. Robust physical-world attacks on deep learning visual classification. In *Proceedings of the IEEE Conference on Computer Vision and Pattern Recognition*, pp. 1625–1634, 2018.

Ian Goodfellow, Jonathon Shlens, and Christian Szegedy. Explaining and harnessing adversarial examples. *2015 ICLR*, arXiv preprint arXiv:1412.6572, 2015.

Ian J Goodfellow, Jonathon Shlens, and Christian Szegedy. Explaining and harnessing adversarial examples. *arXiv preprint arXiv:1412.6572*, 2014.

Kaiming He, Xiangyu Zhang, Shaoqing Ren, and Jian Sun. Deep residual learning for image recognition. In *Proceedings of the IEEE conference on computer vision and pattern recognition*, pp. 770–778, 2016.

Matthias Hein and Maksym Andriushchenko. Formal guarantees on the robustness of a classifier against adversarial manipulation. In *Advances in Neural Information Processing Systems*, pp. 2266–2276, 2017.

Sandy Huang, Nicolas Papernot, Ian J. Goodfellow, Yan Duan, and Pieter Abbeel. Adversarial attacks on neural network policies. In *ICLR (Workshop)*. OpenReview.net, 2017.

Robin Jia and Percy Liang. Adversarial examples for evaluating reading comprehension systems. In *EMNLP*, pp. 2021–2031. Association for Computational Linguistics, 2017.

Daniel Kang, Yi Sun, Dan Hendrycks, Tom Brown, and Jacob Steinhardt. Testing robustness against unforeseen adversaries. *arXiv preprint arXiv:1908.08016*, 2019.

Hamed Karimi, Julie Nutini, and Mark Schmidt. Linear convergence of gradient and proximal-gradient methods under the polyak-łojasiewicz condition. In *Joint European Conference on Machine Learning and Knowledge Discovery in Databases*, pp. 795–811. Springer, 2016.

Sanjay Kariyappa and Moinuddin K Qureshi. Improving adversarial robustness of ensembles with diversity training. *arXiv preprint arXiv:1901.09981*, 2019.

Y. Lecun, L. Bottou, Y. Bengio, and P. Haffner. Gradient-based learning applied to document recognition. *Proceedings of the IEEE*, 86(11):2278–2324, Nov 1998. ISSN 0018-9219. doi: 10.1109/5.726791.

Qi Lei, Lingfei Wu, Pin-Yu Chen, Alexandros G Dimakis, Inderjit S Dhillon, and Michael Witbrock. Discrete adversarial attacks and submodular optimization with applications to text classification. *SysML*, 2019.

Yen-Chen Lin, Zhang-Wei Hong, Yuan-Hong Liao, Meng-Li Shih, Ming-Yu Liu, and Min Sun. Tactics of adversarial attack on deep reinforcement learning agents. In *IJCAI*, pp. 3756–3762. ijcai.org, 2017.

Jiayang Liu, Weiming Zhang, and Nenghai Yu. CAAD 2018: Iterative ensemble adversarial attack. *CoRR*, abs/1811.03456, 2018.

Yanpei Liu, Xinyun Chen, Chang Liu, and Dawn Song. Delving into transferable adversarial examples and black-box attacks. In *ICLR*. OpenReview.net, 2017.

S. Lu, I. Tsaknakis, and M. Hong. Block alternating optimization for non-convex min-max problems: Algorithms and applications in signal processing and communications. 2018. URL http://people.ece.umn.edu/~mhong/Max-Min-Final.pdf.

S. Lu, R. Singh, X. Chen, Y. Chen, and M. Hong. Understand the dynamics of GANs via primal-dual optimization, 2019a. URL https://openreview.net/forum?id=rylIy3R9K7.

Songtao Lu, Ioannis Tsaknakis, and Mingyi Hong. Block alternating optimization for non-convex min-max problems: algorithms and applications in signal processing and communications. In *Proceedings of IEEE International Conference on Acoustics, Speech and Signal Processing (ICASSP)*, 2019b.

Aleksander Madry, Aleksandar Makelov, Ludwig Schmidt, Dimitris Tsipras, and Adrian Vladu. Towards deep learning models resistant to adversarial attacks. *arXiv preprint arXiv:1706.06083*, 2017.

Dongyu Meng and Hao Chen. Magnet: a two-pronged defense against adversarial examples. In *Proceedings of the 2017 ACM SIGSAC Conference on Computer and Communications Security*, pp. 135–147. ACM, 2017.

Jan Hendrik Metzen, Mummadi Chaithanya Kumar, Thomas Brox, and Volker Fischer. Universal adversarial perturbations against semantic image segmentation. In *ICCV*, pp. 2774–2783. IEEE Computer Society, 2017.

Seyed Mohsen Moosavi Dezfooli, Alhussein Fawzi, and Pascal Frossard. Deepfool: a simple and accurate method to fool deep neural networks. In *Proceedings of 2016 IEEE Conference on Computer Vision and Pattern Recognition (CVPR)*, number EPFL-CONF-218057, 2016.

Seyed-Mohsen Moosavi-Dezfooli, Alhussein Fawzi, Omar Fawzi, and Pascal Frossard. Universal adversarial perturbations. In *IEEE Conference on Computer Vision and Pattern Recognition (CVPR)*, pp. 86–94, 2017.

Maher Nouiehed, Maziar Sanjabi, Jason D Lee, and Meisam Razaviyayn. Solving a class of non-convex min-max games using iterative first order methods. *arXiv preprint arXiv:1902.08297*, 2019.

Tianyu Pang, Kun Xu, Chao Du, Ning Chen, and Jun Zhu. Improving adversarial robustness via promoting ensemble diversity. *arXiv preprint arXiv:1901.08846*, 2019.

Nicolas Papernot, Patrick McDaniel, Somesh Jha, Matt Fredrikson, Z Berkay Celik, and Ananthram Swami. The limitations of deep learning in adversarial settings. In *Security and Privacy (EuroS&P), 2016 IEEE European Symposium on*, pp. 372–387. IEEE, 2016a.

Nicolas Papernot, Patrick McDaniel, Xi Wu, Somesh Jha, and Ananthram Swami. Distillation as a defense to adversarial perturbations against deep neural networks. In *Security and Privacy (SP), 2016 IEEE Symposium on*, pp. 582–597. IEEE, 2016b.

Nicolas Papernot, Patrick McDaniel, Ian Goodfellow, Somesh Jha, Z Berkay Celik, and Ananthram Swami. Practical black-box attacks against machine learning. In *Proceedings of the 2017 ACM on Asia Conference on Computer and Communications Security*, pp. 506–519. ACM, 2017.

Neal Parikh, Stephen Boyd, et al. Proximal algorithms. *Foundations and Trends® in Optimization*, 1 (3):127–239, 2014.

Q. Qian, S. Zhu, J. Tang, R. Jin, B. Sun, and H. Li. Robust optimization over multiple domains. *CoRR*, abs/1805.07588, 2018. URL http://arxiv.org/abs/1805.07588.

H. Rafique, M. Liu, Q. Lin, and T. Yang. Non-convex min-max optimization: Provable algorithms and applications in machine learning. *arXiv preprint arXiv:1810.02060*, 2018.

Ali Shafahi, Mahyar Najibi, Zheng Xu, John P. Dickerson, Larry S. Davis, and Tom Goldstein. Universal adversarial training. *CoRR*, abs/1811.11304, 2018.

Karen Simonyan and Andrew Zisserman. Very deep convolutional networks for large-scale image recognition. In *ICLR*, 2015.

Jost Tobias Springenberg, Alexey Dosovitskiy, Thomas Brox, and Martin A. Riedmiller. Striving for simplicity: The all convolutional net. In *ICLR (Workshop)*, 2015.

Dong Su, Huan Zhang, Hongge Chen, Jinfeng Yi, Pin-Yu Chen, and Yupeng Gao. Is robustness the cost of accuracy?–a comprehensive study on the robustness of 18 deep image classification models. In *Proceedings of the European Conference on Computer Vision (ECCV)*, pp. 631–648, 2018.

Christian Szegedy, Wojciech Zaremba, Ilya Sutskever, Joan Bruna, Dumitru Erhan, Ian Goodfellow, and Rob Fergus. Intriguing properties of neural networks. *arXiv preprint arXiv:1312.6199*, 2013.

Christian Szegedy, Wei Liu, Yangqing Jia, Pierre Sermanet, Scott E. Reed, Dragomir Anguelov, Dumitru Erhan, Vincent Vanhoucke, and Andrew Rabinovich. Going deeper with convolutions. In *CVPR*, pp. 1–9. IEEE Computer Society, 2015.

F. Tramèr, A. Kurakin, N. Papernot, I. Goodfellow, D. Boneh, and P. McDaniel. Ensemble adversarial training: Attacks and defenses. *2018 ICLR*, arXiv preprint arXiv:1705.07204, 2018.

Florian Tramèr and Dan Boneh. Adversarial training and robustness for multiple perturbations. *arXiv preprint arXiv:1904.13000*, 2019.

Florian Tramèr, Nicolas Papernot, Ian Goodfellow, Dan Boneh, and Patrick McDaniel. The space of transferable adversarial examples. *arXiv preprint arXiv:1704.03453*, 2017.

Cihang Xie, Jianyu Wang, Zhishuai Zhang, Zhou Ren, and Alan Yuille. Mitigating adversarial effects through randomization. *arXiv preprint arXiv:1711.01991*, 2017.

Kaidi Xu, Sijia Liu, Pu Zhao, Pin-Yu Chen, Huan Zhang, Quanfu Fan, Deniz Erdogmus, Yanzhi Wang, and Xue Lin. Structured adversarial attack: Towards general implementation and better interpretability. In *International Conference on Learning Representations*, 2019. URL https://openreview.net/forum?id=BkgzniCqY7.

Weilin Xu, David Evans, and Yanjun Qi. Feature squeezing: Detecting adversarial examples in deep neural networks. In *NDSS*. The Internet Society, 2018.

Sergey Zagoruyko and Nikos Komodakis. Wide residual networks. In *BMVC*. BMVA Press, 2016.

Zhengli Zhao, Dheeru Dua, and Sameer Singh. Generating natural adversarial examples. In *ICLR*. OpenReview.net, 2018.

CONTENTS

LIST OF FIGURES

LIST OF TABLES

A   PROOF OF LEMMA 1

Lemma 1. *Problem* (10) *is equivalent to*

$$\underset{\boldsymbol{\theta}}{\text{minimize}}\ \mathbb{E}_{(\mathbf{x},\mathbf{y})\in\mathcal{D}}\ \underset{\mathbf{w}\in\mathcal{P},\{\boldsymbol{\delta}_i\in\mathcal{X}_i\}}{\text{maximize}}\ \sum_{i=1}^{K}w_i f_{\text{tr}}(\boldsymbol{\theta},\boldsymbol{\delta}_i;\mathbf{x},y),$$

where $\mathbf{w}\in\mathbb{R}^K$ *represent domain weights, and* $\mathcal{P}$ *has been defined in* (1).

Proof of Lemma 1:

Similar to (1), problem (10) is equivalent to

$$\underset{\boldsymbol{\theta}}{\text{minimize}}\ \mathbb{E}_{(\mathbf{x},\mathbf{y})\in\mathcal{D}}\ \underset{\mathbf{w}\in\mathcal{P}}{\text{maximize}}\sum_{i=1}^{K}w_i F_i(\boldsymbol{\theta}). \tag{18}$$

Recall that $F_i(\boldsymbol{\theta}) := \text{maximize}_{\boldsymbol{\delta}_i\in\mathcal{X}_i}\ f_{\text{tr}}(\boldsymbol{\theta},\boldsymbol{\delta}_i;\mathbf{x},y)$, problem can then be written as

$$\underset{\boldsymbol{\theta}}{\text{minimize}}\ \mathbb{E}_{(\mathbf{x},\mathbf{y})\in\mathcal{D}}\ \underset{\mathbf{w}\in\mathcal{P}}{\text{maximize}}\sum_{i=1}^{K}[w_i\ \underset{\boldsymbol{\delta}_i\in\mathcal{X}_i}{\text{maximize}}\ f_{\text{tr}}(\boldsymbol{\theta},\boldsymbol{\delta}_i;\mathbf{x},y)]. \tag{19}$$

According to proof by contradiction, it is clear that problem (19) is equivalent to

$$\underset{\boldsymbol{\theta}}{\text{minimize}}\ \mathbb{E}_{(\mathbf{x},\mathbf{y})\in\mathcal{D}}\ \underset{\mathbf{w}\in\mathcal{P},\{\boldsymbol{\delta}_i\in\mathcal{X}_i\}}{\text{maximize}}\ \sum_{i=1}^{K}w_i f_{\text{tr}}(\boldsymbol{\theta},\boldsymbol{\delta}_i;\mathbf{x},y). \tag{20}$$

$\square$

B   PROOF OF PROPOSITION 1

Proposition 1. *Given a point* $\mathbf{a}\in\mathbb{R}^d$ *and a constraint set* $\mathcal{X}=\{\boldsymbol{\delta}|\|\boldsymbol{\delta}\|_p\le\epsilon,\check{\mathbf{c}}\le\boldsymbol{\delta}\le\hat{\mathbf{c}}\}$, *the Euclidean projection* $\boldsymbol{\delta}^*=\text{proj}_{\mathcal{X}}(\mathbf{a})$ *has the closed-form solution when* $p\in\{0,1,2\}$.

1) If $p=1$, *then* $\boldsymbol{\delta}^*$ *is given by*

$$\delta_i^*=\begin{cases} P_{[\check{c}_i,\hat{c}_i]}(a_i) & \sum_{i=1}^{d}|P_{[\check{c}_i,\hat{c}_i]}(a_i)|\le\epsilon \\ P_{[\check{c}_i,\hat{c}_i]}(\text{sign}(a_i)\max\{|a_i|-\lambda_1,0\}) & \text{otherwise}, \end{cases} \tag{21}$$

where $\mathbf{x}_i$ *denotes the ith element of a vector* $\mathbf{x}$; $P_{[\check{c}_i,\hat{c}_i]}(\cdot)$ *denotes the clip function over the interval* $[\check{c}_i,\hat{c}_i]$; $\text{sign}(x)=1$ *if* $x\ge 0$, *otherwise* 0; $\lambda_1\in(0,\max_i|a_i|-\epsilon/d]$ *is the root of* $\sum_{i=1}^{d}|P_{[\check{c}_i,\hat{c}_i]}(\text{sign}(a_i)\max\{|a_i|-\lambda_1,0\})|=\epsilon$.

2) If $p=2$, *then* $\boldsymbol{\delta}^*$ *is given by*

$$\delta_i^*=\begin{cases} P_{[\check{c}_i,\hat{c}_i]}(a_i) & \sum_{i=1}^{d}(P_{[\check{c}_i,\hat{c}_i]}(a_i))^2\le\epsilon^2 \\ P_{[\check{c}_i,\hat{c}_i]}(a_i/(\lambda_2+1)) & \text{otherwise}, \end{cases} \tag{22}$$

where $\lambda_2\in(0,\|\mathbf{a}\|_2/\epsilon-1]$ *is the root of* $\sum_{i=1}^{d}(P_{[\check{c}_i,\hat{c}_i]}(a_i/(\lambda_2+1)))^2=\epsilon^2$.

3) If $p=0$ *and* $\epsilon\in\mathbb{N}_+$, *then* $\boldsymbol{\delta}^*$ *is given by*

$$\delta_i^*=\begin{cases} \delta_i' & \eta_i\ge[\boldsymbol{\eta}]_\epsilon \\ 0 & \text{otherwise}, \end{cases} \qquad \eta_i=\begin{cases} \sqrt{2a_i\check{c}_i-\check{c}_i^2} & a_i<\check{c}_i \\ \sqrt{2a_i\hat{c}_i-\hat{c}_i^2} & a_i>\hat{c}_i \\ |a_i| & \text{otherwise}. \end{cases} \tag{23}$$

where $[\boldsymbol{\eta}]_\epsilon$ *denotes the* ϵ-*th largest element of* $\boldsymbol{\eta}$, *and* $\delta_i'=P_{[\check{c}_i,\hat{c}_i]}(a_i)$.

Proof of Proposition 1:

ℓ_1 **norm** When we find the Euclidean projection of $\mathbf{a}$ onto the set $\mathcal{X}$, we solve

$$\begin{array}{ll} \underset{\boldsymbol{\delta}}{\text{minimize}} & \frac{1}{2}\|\boldsymbol{\delta} - \mathbf{a}\|_2^2 + I_{[\check{\mathbf{c}},\hat{\mathbf{c}}]}(\boldsymbol{\delta}) \\ \text{subject to} & \|\boldsymbol{\delta}\|_1 \leq \epsilon, \end{array} \tag{24}$$

where $I_{[\check{\mathbf{c}},\hat{\mathbf{c}}]}(\cdot)$ is the indicator function of the set $[\check{\mathbf{c}}, \hat{\mathbf{c}}]$. The Langragian of this problem is

$$L = \frac{1}{2}\|\boldsymbol{\delta} - \mathbf{a}\|_2^2 + I_{[\check{\mathbf{c}},\hat{\mathbf{c}}]}(\boldsymbol{\delta}) + \lambda_1(\|\boldsymbol{\delta}\|_1 - \epsilon) \tag{25}$$

$$= \sum_{i=1}^{d} (\frac{1}{2}(\delta_i - a_i)^2 + \lambda_1|\delta_i| + I_{[\check{c}_i,\hat{c}_i]}(\delta_i)) - \lambda_1\epsilon. \tag{26}$$

The minimizer $\boldsymbol{\delta}^*$ minimizes the Lagrangian, it is obtained by elementwise soft-thresholding

$$\delta_i^* = P_{[\check{c}_i,\hat{c}_i]}(\text{sign}(a_i) \max\{|a_i| - \lambda_1, 0\}).$$

where $\mathbf{x}_i$ is the ith element of a vector $\mathbf{x}$, $P_{[\check{c}_i,\hat{c}_i]}(\cdot)$ is the clip function over the interval $[\check{c}_i, \hat{c}_i]$.
The primal, dual feasibility and complementary slackness are

$$\lambda_1 = 0, \|\boldsymbol{\delta}\|_1 = \sum_{i=1}^{d} |\delta_i| = \sum_{i=1}^{d} |P_{[\check{c}_i,\hat{c}_i]}(a_i)| \leq \epsilon \tag{27}$$

$$\text{or } \lambda_1 > 0, \|\boldsymbol{\delta}\|_1 = \sum_{i=1}^{d} |\delta_i| = \sum_{i=1}^{d} |P_{[\check{c}_i,\hat{c}_i]}(\text{sign}(a_i) \max\{|a_i| - \lambda_1, 0\})| = \epsilon. \tag{28}$$

If $\sum_{i=1}^{d} |P_{[\check{c}_i,\hat{c}_i]}(a_i)| \leq \epsilon$, $\delta_i^* = P_{[\check{c}_i,\hat{c}_i]}(a_i)$. Otherwise $\delta_i^* = P_{[\check{c}_i,\hat{c}_i]}(\text{sign}(a_i) \max\{|a_i| - \lambda_1, 0\})$, where λ_1 is given by the root of the equation $\sum_{i=1}^{d} |P_{[\check{c}_i,\hat{c}_i]}(\text{sign}(a_i) \max\{|a_i| - \lambda_1, 0\})| = \epsilon$. Bisection method can be used to solve the above equation for λ_1, starting with the initial interval $(0, \max_i |a_i| - \epsilon/d]$. Since $\sum_{i=1}^{d} |P_{[\check{c}_i,\hat{c}_i]}(\text{sign}(a_i) \max\{|a_i| - 0, 0\})| = \sum_{i=1}^{d} |P_{[\check{c}_i,\hat{c}_i]}(a_i)| > \epsilon$ in this case, and $\sum_{i=1}^{d} |P_{[\check{c}_i,\hat{c}_i]}(\text{sign}(a_i) \max\{|a_i| - \max_i |a_i| + \epsilon/d, 0\})| \leq \sum_{i=1}^{d} |P_{[\check{c}_i,\hat{c}_i]}(\text{sign}(a_i)(\epsilon/d))| \leq \sum_{i=1}^{d}(\epsilon/d) = \epsilon$.

ℓ_2 **norm** When we find the Euclidean projection of $\mathbf{a}$ onto the set $\mathcal{X}$, we solve

$$\begin{array}{ll} \underset{\boldsymbol{\delta}}{\text{minimize}} & \|\boldsymbol{\delta} - \mathbf{a}\|_2^2 + I_{[\check{\mathbf{c}},\hat{\mathbf{c}}]}(\boldsymbol{\delta}) \\ \text{subject to} & \|\boldsymbol{\delta}\|_2^2 \leq \epsilon^2, \end{array} \tag{29}$$

where $I_{[\check{\mathbf{c}},\hat{\mathbf{c}}]}(\cdot)$ is the indicator function of the set $[\check{\mathbf{c}}, \hat{\mathbf{c}}]$. The Langragian of this problem is

$$L = \|\boldsymbol{\delta} - \mathbf{a}\|_2^2 + I_{[\check{\mathbf{c}},\hat{\mathbf{c}}]}(\boldsymbol{\delta}) + \lambda_2(\|\boldsymbol{\delta}\|_2^2 - \epsilon^2) \tag{30}$$

$$= \sum_{i=1}^{d} ((\delta_i - a_i)^2 + \lambda_2\delta_i^2 + I_{[\check{c}_i,\hat{c}_i]}(\delta_i)) - \lambda_2\epsilon^2. \tag{31}$$

The minimizer $\boldsymbol{\delta}^*$ minimizes the Lagrangian, it is

$$\delta_i^* = P_{[\check{c}_i,\hat{c}_i]}(\frac{1}{\lambda_2 + 1} a_i).$$

The primal, dual feasibility and complementary slackness are

$$\lambda_2 = 0, \|\boldsymbol{\delta}\|_2^2 = \sum_{i=1}^{d} \delta_i^2 = \sum_{i=1}^{d} (P_{[\check{c}_i,\hat{c}_i]}(a_i))^2 \leq \epsilon^2 \tag{32}$$

$$\text{or } \lambda_2 > 0, \|\boldsymbol{\delta}\|_2^2 = \sum_{i=1}^{d} \delta_i^2 = (P_{[\check{c}_i,\hat{c}_i]}(\frac{1}{\lambda_2 + 1} a_i))^2 = \epsilon^2. \tag{33}$$

If $\sum_{i=1}^{d}(P_{[\check{c}_i,\hat{c}_i]}(a_i))^2 \leq \epsilon^2$, $\delta_i^* = P_{[\check{c}_i,\hat{c}_i]}(a_i)$. Otherwise $\delta_i^* = P_{[\check{c}_i,\hat{c}_i]}\left(\frac{1}{\lambda_2+1}a_i\right)$, where λ_2 is given by the root of the equation $\sum_{i=1}^{d}(P_{[\check{c}_i,\hat{c}_i]}(\frac{1}{\lambda_2+1}a_i))^2 = \epsilon^2$. Bisection method can be used to solve the above equation for λ_2, starting with the initial interval $(0, \sqrt{\sum_{i=1}^{d}(a_i)^2}/\epsilon - 1]$. Since $\sum_{i=1}^{d}(P_{[\check{c}_i,\hat{c}_i]}(\frac{1}{0+1}a_i))^2 = \sum_{i=1}^{d}(P_{[\check{c}_i,\hat{c}_i]}(a_i))^2 > \epsilon^2$ in this case, and $\sum_{i=1}^{d}(P_{[\check{c}_i,\hat{c}_i]}(\frac{1}{\lambda_2+1}a_i))^2 = \sum_{i=1}^{d}(P_{[\check{c}_i,\hat{c}_i]}(\epsilon a_i/\sqrt{\sum_{i=1}^{d}(a_i)^2}))^2 \leq \epsilon^2 \sum_{i=1}^{d}(a_i)^2/(\sqrt{\sum_{i=1}^{d}(a_i)^2})^2 = \epsilon^2$.

ℓ_0 **norm** For ℓ_0 norm in $\mathcal{X}$, it is independent to the box constraint. So we can clip **a** to the box constraint first, which is $\delta_i' = P_{[\check{c}_i,\hat{c}_i]}(a_i)$, and then project it onto ℓ_0 norm.

We find the additional Euclidean distance of every element in **a** and zero after they are clipped to the box constraint, which is

$$\eta_i = \begin{cases} \sqrt{a_i^2 - (a_i - \check{c}_i)^2} & a_i < \check{c}_i \\ \sqrt{a_i^2 - (a_i - \hat{c}_i)^2} & a_i > \hat{c}_i \\ |a_i| & \text{otherwise.} \end{cases} \tag{34}$$

It can be equivalently written as

$$\eta_i = \begin{cases} \sqrt{2a_i\check{c}_i - \check{c}_i^2} & a_i < \check{c}_i \\ \sqrt{2a_i\hat{c}_i - \hat{c}_i^2} & a_i > \hat{c}_i \\ |a_i| & \text{otherwise.} \end{cases} \tag{35}$$

To derive the Euclidean projection onto ℓ_0 norm, we find the ϵ-th largest element in $\boldsymbol{\eta}$ and call it $[\boldsymbol{\eta}]_\epsilon$. We keep the elements whose corresponding η_i is above or equals to ϵ-th, and set rest to zeros. The closed-form solution is given by

$$\delta_i^* = \begin{cases} \delta_i' & \eta_i \geq [\boldsymbol{\eta}]_\epsilon \\ 0 & \text{otherwise.} \end{cases} \tag{36}$$

$\square$

Difference to (Hein & Andriushchenko, 2017, Proposition 4.1). We remark that Hein & Andriushchenko (2017) discussed a relevant problem of generating ℓ_p-norm based adversarial examples under box and linearized classification constraints. It was shown in (Hein & Andriushchenko, 2017, Proposition 4.1) that the problem is convex and the solution can be derived using KKT conditions. However, Proposition 1 in our paper is different from (Hein & Andriushchenko, 2017, Proposition 4.1). First, we place ℓ_p norm as a hard constraint rather than minimizing it in the objective function. This difference will make our Lagrangian function more involved with a newly introduced non-negative Lagrangian multiplier. Second, the problem of our interest is projection onto the intersection of box and ℓ_p constraints. Such a projection step can then be combined with an attack loss (no need of linearization) for generating adversarial examples. Third, we cover the case of ℓ_0 norm.

C EXPERIMENT SETUP

C.1 MODEL ARCHITECTURES AND TRAINING DETAILS

For a comprehensive evaluation of proposed algorithms, we adopt a set of diverse DNN models (Model A to H), including multi-layer perceptrons (MLP), All-CNNs Springenberg et al. (2015), LeNet Lecun et al. (1998), LeNetV2[3], VGG16 Simonyan & Zisserman (2015), ResNet50 He et al. (2016), Wide-ResNet Madry et al. (2017) and GoogLeNet Szegedy et al. (2015). For the last four models, we use the exact same architecture as original papers and evaluate them only on CIFAR-10 dataset. The details for model architectures are provided in Table A1. For compatibility with our framework, we implement and train these models based on the strategies adopted in pytorch-cifar[4] and achieve comparable performance on clean images; see Table A2. To foster reproducibility, all the trained models are publicly accessible in the anonymous link. Specifically, we trained MNIST

---

[3] An enhanced version of original LeNet with more layers and units (see Table A1 Model D).
[4] https://github.com/kuangliu/pytorch-cifar

classifiers for 50 epochs with Adam and a constant learning rate of 0.001. For CIFAR-10 classifers, the models are trained for 250 epochs with SGD (using 0.8 nesterov momentum, weight decay $5e^{-4}$). The learning rate is reduced at epoch 100 and 175 with a decay rate of 0.1. The initial learning rate is set as 0.01 for models {A, B, C, D, H} and 0.1 for {E, F, G}. Note that no data augmentation is employed in the training.

Table A1: Neural network architectures used on the MNIST and CIFAR-10 dataset. Conv: convolutional layer, FC: fully connected layer, Globalpool: global average pooling layer.

A (MLP)	**B** (All-CNNs, 2015)	**C** (LeNet, 1998)	**D** (LeNetV2)
FC(128) + Relu	Conv([32, 64], 3, 3) + Relu	Conv(6, 5, 5) + Relu	Conv(32, 3, 3) + Relu
FC(128) + Relu	Conv(128, 3, 3) + Dropout(0.5)	Maxpool(2, 2)	Maxpool(2, 2)
FC(64) + Relu	Conv([128, 128], 3, 3) + Relu	Conv(16, 5, 5) + Relu	Conv(64, 3, 3) + Relu
FC(10)	Conv(128, 3, 3) + Dropout(0.5)	Maxpool(2, 2)	Maxpool(2, 2)
Softmax	Conv(128, 3, 3) + Relu	FC(120) + Relu	FC(128) + Relu
	Conv(128, 1, 1) + Relu	FC(84) + Relu	Dropout(0.25)
	Conv(10, 1, 1) + Globalpool	FC(10)	FC(10)
	Softmax	Softmax	Softmax
E (VGG16, 2015)	**F** (ResNet50, 2016)	**G** (Wide-ResNet, 2017)	**H** (GoogLeNet, 2015)

Table A2: Clean test accuracy of DNN models on MNIST and CIFAR-10. We roughly derive the model robustness by attacking models separately using FGSM Goodfellow et al. (2014). The adversarial examples are generated by FGSM ℓ_∞-attack ($\epsilon = 0.2$).

MNIST			CIFAR-10					
Model	Acc.	FGSM	Model	Acc.	FGSM	Model	Acc.	FGSM
A: MLP	98.20%	18.92%	A: MLP	55.36%	11.25%	E: VGG16	87.57%	10.83%
B: All-CNNs	99.49%	50.95%	B: All-CNNs	84.18%	9.89%	F: ResNet50	88.11%	10.73%
C: LeNet	99.25%	63.23%	C: LeNet	64.95%	14.45%	G: Wide-ResNet	91.67%	15.78%
D: LeNetV2	99.33%	56.36%	D: LeNetV2	74.89%	9.77%	H: GoogLeNet	90.92%	9.91%

C.2 CRAFTING ADVERSARIAL EXAMPLES

We adopt variant C&W loss in APGD/PGD as suggested in Madry et al. (2017); Carlini & Wagner (2017) with a confidence parameter $\kappa = 50$. Cross-entropy loss is also supported in our implementation. The adversarial examples are generated by 20-step PGD/APGD unless otherwise stated (e.g., 50 steps for ensemble attacks). Note that proposed algorithms are robust and will not be affected largely by the choices of hyperparameters (α, β, γ). In consequence, we do not finely tune the parameters on the validation set. Specifically, The learning rates α, β and regularization factor γ for Table 1 are set as - (a) MNIST: $\ell_0 : \alpha = 1, \beta = \frac{1}{100}, \gamma = 7$, $\ell_1 : \alpha = \frac{1}{4}, \beta = \frac{1}{100}, \gamma = 5$, $\ell_2 : \alpha = \frac{1}{10}, \beta = \frac{1}{100}, \gamma = 3$; $\ell_\infty : \alpha = \frac{1}{4}, \beta = \frac{1}{50}, \gamma = 3$; (b) CIFAR-10: $\ell_0 : \alpha = 1, \beta = \frac{1}{150}, \gamma = 1, \ell_1 : \alpha = \frac{1}{4}, \beta = \frac{1}{100}, \gamma = 5, \ell_2 : \alpha = \frac{1}{8}, \beta = \frac{1}{100}, \gamma = 3$; $\ell_\infty : \alpha = \frac{1}{5}, \beta = \frac{1}{50}, \gamma = 6$.

Due to varying model robustness on different datasets, the perturbation magnitudes ϵ are set separately Carlini et al. (2019). For universal perturbation experiments, the ϵ are set as 0.2 (A, B), 0.3 (C) and 0.25 (D) on MNIST; 0.02 (B, H), 0.35 (E) and 0.05 (D) on CIFAR-10. For generalized AT, the models on MNIST are trained following the same rules in last section, except that training epochs are prolonged to 350 and adversarial examples are crafted for assisting the training with a ratio of 0.5. Our experiment setup is based on CleverHans package[5] and Carlini and Wagner's framework[6].

C.3 DETAILS OF CONDUCTED DATA TRANSFORMATIONS

To demonstrate the effectiveness of APGD in generating robust adversarial examples against multiple transformations, we adopt a series of common transformations, including a&b) flipping images

---

[5] https://github.com/tensorflow/cleverhans
[6] https://github.com/carlini/nn_robust_attacks

horizontally (*flh*) and vertically (*flv*); c) adjusting image brightness (*bri*); d) performing gamma correction (*gam*), e) cropping and re-sizing images (*crop*); f) rotating images (*rot*).

Moreover, both deterministic and stochastic transformations are considered in our experiments. In particular, Table 3 and Table A6 are deterministic settings - *rot*: rotating images 30 degree clockwise; *crop*: cropping images in the center (0.8×0.8) and resizing them to 32×32; *bri*: adjusting the brightness of images with a scale of 0.1; *gam*: performing gamma correction with a value of 1.3. Differently, in Table A5, we introduce randomness for drawing samples from the distribution - *rot*: rotating images randomly from -10 to 10 degree; *crop*: cropping images in the center randomly (from 0.6 to 1.0); other transformations are done with a probability of 0.8. In experiments, we adopt `tf.image` API [7] for processing the images.

D SUPPLEMENTARY RESULTS - ROBUST ADVERSARIAL ATTACKS

D.1 ENSEMBLE ATTACK OVER MULTIPLE MODELS

Table A3 shows the performance of average (ensemble PGD Liu et al. (2018)) and min-max (APGD) strategies for attacking model ensembles. Our min-max approach results in 15.69% averaged improvement on ASR_{all} over models {A, E, F, H} on CIFAR-10.

Table A3: Comparison of average and min-max (APGD) ensemble attack over four models on CIFAR-10. Acc (%) represents the test accuracy of classifiers on adversarial examples. The learning rates α, β and regularization factor γ are set as - $\ell_0 : \alpha = 1, \beta = \frac{1}{150}, \gamma = 1, \ell_1 : \alpha = \frac{1}{4}, \beta = \frac{1}{100}, \gamma = 5, \ell_2 : \alpha = \frac{1}{8}, \beta = \frac{1}{100}, \gamma = 3; \ell_\infty : \alpha = \frac{1}{5}, \beta = \frac{1}{50}, \gamma = 6$. The attack iteration for APGD is set as 50.

Box constraint	Opt.	Acc_A	Acc_E	Acc_F	Acc_H	ASR_{all}	Lift ($\uparrow$)
ℓ_0 ($\epsilon = 70$)	*avg.*	27.38	6.33	7.18	6.99	66.56	-
	min max	19.38	8.72	9.48	8.94	**73.83**	**10.92%**
ℓ_1 ($\epsilon = 30$)	*avg.*	30.90	2.06	1.85	1.84	66.23	-
	min max	12.56	3.21	2.70	2.72	**83.13**	**25.52%**
ℓ_2 ($\epsilon = 1.5$)	*avg.*	20.87	1.75	1.21	1.54	76.41	-
	min max	10.26	3.15	2.24	2.37	**84.99**	**11.23%**
ℓ_∞ ($\epsilon = 0.03$)	*avg.*	25.75	2.59	1.66	2.27	70.54	-
	min max	13.47	3.79	3.15	3.48	**81.17**	**15.07%**

D.2 COMPARISON WITH HEURISTIC WEIGHTING SCHEMES

To further demonstrate the effectiveness of self-adjusted weighting factors in proposed min-max framework, we compare with heuristic weighting schemes in Table A4. Specifically, with the prior knowledge of robustness of given models (C > D > A > B), we devised several heuristic baselines including: (a) w_{c+d}: ensemble PGD on models C and D only; (b) w_{a+c+d}: ensemble PGD on models A, C and D only; (c) w_{clip}: clipped version of C&W loss (threshold $\beta = 40$) to balance model weights in optimization as suggested in Shafahi et al. (2018); (d) w_{prior}: larger weights on the more robust models, $w_{prior} = [w_A, w_B, w_C, w_D] = [0.2, 0.1, 0.4, 0.3]$; (e) w_{static}: the converged mean weights of min-max (APGD) ensemble attack. For ℓ_2 ($\epsilon = 3.0$) and ℓ_∞ ($\epsilon = 0.2$) attacks, $w_{static} = [w_A, w_B, w_C, w_D]$ are $[0.209, 0.046, 0.495, 0.250]$ and $[0.080, 0.076, 0.541, 0.303]$, respectively.

Table A4 shows that our min-max approach outperforms all static heuristic weighting schemes by a large margin. Specifically, our min-max APGD also achieves significant improvement compared to w_{static} setting, where the converged optimal weights are statically (i.e., invariant w.r.t different images and attack procedure) adopted. It again verifies the benefits of proposed min-max approach by automatically learning the weights for different examples during the process of ensemble attack generation (see Figure 1c).

---

[7] https://www.tensorflow.org/api_docs/python/tf/image

Table A4: Comparison of average, min-max (APGD) ensemble attack and some heuristic weighting schemes over four models on MNIST. Acc (%) represents the test accuracy of classifiers on adversarial examples. w_{c+d} and w_{a+c+d}: average ensemble attack over models {C, D} and {A, C, D}; w_{clip}: clipped version of C&W loss (Shafahi et al., 2018). w_{prior}: larger weights on the models that are more difficult to attack - $[w_A, w_B, w_C, w_D] = [0.2, 0.1, 0.4, 0.3]$; w_{static}: converged mean weights (over all data) in $\min\max$ ensemble attack. The experimental setting is the same as Table 1.

Box constraint	Opt.	Acc_A	Acc_B	Acc_C	Acc_D	ASR_{avg}	ASR_{all}	Lift ($\uparrow$)
	$avg.$	6.88	0.03	26.28	14.50	88.08	69.12	-
	w_{c+d}	69.03	14.58	5.11	0.34	77.74	28.65	-58.56%
	w_{a+c+d}	1.34	24.53	11.69	2.79	89.91	67.45	-2.42%
ℓ_2 ($\epsilon = 3.0$)	w_{clip}	2.70	0.02	12.69	4.13	95.12	85.33	23.45%
	w_{prior}	6.28	0.05	6.78	2.65	96.06	88.25	27.68%
	w_{static}	4.52	0.27	3.35	4.15	96.93	90.53	30.98%
	$\min\max$	1.51	0.89	3.50	2.06	**98.01**	**95.31**	**37.89%**
	$avg.$	1.05	0.07	41.10	35.03	80.69	48.17	-
	w_{c+d}	60.37	19.55	15.10	1.87	75.78	29.32	-39.13%
	w_{a+c+d}	0.46	21.57	25.36	13.84	84.69	53.39	10.84%
ℓ_∞ ($\epsilon = 0.2$)	w_{clip}	0.66	0.03	23.43	13.23	90.66	71.54	48.52%
	w_{prior}	1.57	0.24	17.67	13.74	91.70	74.34	54.33%
	w_{static}	10.58	0.39	9.28	10.05	92.43	77.84	61.59%
	$\min\max$	2.47	0.37	7.39	5.81	**95.99**	**90.16**	**87.17%**

D.3 ROBUST ADVERSARIAL ATTACK OVER DATA TRANSFORMATIONS

Table A5 and A6 compare the performance of average (EOT Athalye et al. (2018a)) and min-max (APGD) strategies. Our approach results in 4.31% and 8.22% averaged lift over four models {A, B, C, D} on CIFAR-10 under given stochastic and deterministic transformation sets.

Table A5: Comparison of average and min-max optimization on robust attack over multiple data transformations on CIFAR-10. Note that all data transformations are conducted stochastically with a probability of 0.8, except for *crop* which randomly crops a central area from original image and re-size it into 32×32. The adversarial examples are generated by 20-step ℓ_∞-APGD ($\epsilon = 0.03$) with $\alpha = \frac{1}{2}, \beta = \frac{1}{100}$ and $\gamma = 10$.

Model	Opt.	Acc_{ori}	Acc_{flh}	Acc_{flv}	Acc_{bri}	Acc_{crop}	ASR_{avg}	ASR_{gp}	Lift ($\uparrow$)
A	$avg.$	11.55	21.60	13.64	12.30	22.37	83.71	55.97	-
	$\min\max$	13.06	18.90	13.43	13.90	20.27	84.09	**59.17**	**5.72%**
B	$avg.$	6.74	11.55	10.33	6.59	18.21	89.32	69.52	-
	$\min\max$	8.19	11.13	10.31	8.31	16.29	89.15	**71.18**	**2.39%**
C	$avg.$	8.23	17.47	13.93	8.54	18.83	86.60	58.85	-
	$\min\max$	9.68	13.45	13.41	9.95	18.23	87.06	**61.63**	**4.72%**
D	$avg.$	8.67	19.75	11.60	8.46	19.35	86.43	60.96	-
	$\min\max$	10.43	16.41	12.14	10.15	17.64	86.65	**63.64**	**4.40%**

Table A6: Comparison of average and min-max optimization on robust attack over multiple data transformations on CIFAR-10. Here a new rotation (*rot*) transformation is introduced, where images are rotated 30 degrees clockwise. Note that all data transformations are conducted with a probability of 1.0. The adversarial examples are generated by 20-step ℓ_∞-APGD ($\epsilon = 0.03$) with $\alpha = \frac{1}{2}, \beta = \frac{1}{100}$ and $\gamma = 10$.

Model	Opt.	Acc_{ori}	Acc_{flh}	Acc_{flv}	Acc_{bri}	Acc_{gam}	Acc_{crop}	Acc_{rot}	ASR_{avg}	ASR_{gp}	Lift ($\uparrow$)
A	$avg.$	11.06	22.37	14.81	12.32	10.92	20.40	15.89	84.60	49.24	-
	$\min\max$	13.51	18.84	14.03	15.20	13.00	18.03	14.79	84.66	**52.31**	**6.23%**
B	$avg.$	5.55	11.96	9.97	5.63	5.94	16.42	11.47	90.44	65.18	-
	$\min\max$	6.75	9.13	10.56	6.72	7.11	12.23	10.80	90.96	**70.38**	**7.98%**
C	$avg.$	7.65	22.30	15.82	8.17	8.07	15.44	15.09	86.78	49.67	-
	$\min\max$	9.05	15.10	14.57	9.57	9.31	14.11	14.23	87.72	**55.37**	**11.48%**
D	$avg.$	8.22	20.88	13.49	7.91	8.71	16.33	14.98	87.07	53.52	-
	$\min\max$	10.17	14.65	13.62	10.03	10.35	14.36	13.82	87.57	**57.36**	**7.17%**

D.4 SENSITIVITY ANALYSIS OF REGULARIZER ON PROBABILITY SIMPLEX

To further explore the utility of quadratic regularizer on the probability simplex in proposed min-max framework, we conducted sensitivity analysis on γ and show how the proposed regularization affects the eventual performance (Figure A1) taking ensemble attack as an example. The experimental setting is the same as Table 1 except for altering the value of γ from 0 to 10. Figure A1 shows that too small or too large γ leads to relative weak performance due to the unstable convergence and penalizing too much for average case. When γ is around 4, APGD will achieve the best performance so we adopted this value in the experiments (Table 1). Moreover, when $\gamma \to \infty$, the regularizer term dominates the optimization objective and it becomes the average case.
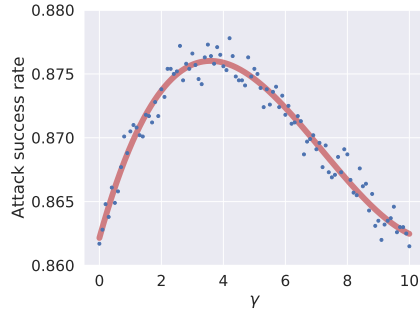
Figure A1: Sensitivity analysis of the regularizer $\frac{\gamma}{2}\|\mathbf{w} - \mathbf{1}/K\|_2^2$ on the probability simplex.

E   SUPPLEMENTARY RESULTS - ADVERSARIAL TRAINING AGAINST MULTIPLE TYPES OF ADVERSARIAL ATTACKS

E.1   ROBUSTNESS EVALUATION

Figure A2 presents "overall robustness" comparison of our min-max generalized AT scheme and vanilla AT with single type of attacks (ℓ_∞ and ℓ_2) on MNIST (LeNet). Similarly, our min-max training scheme leads to a higher "overall robustness" measured by S_ϵ. In practice, due to the lacking knowledge of the strengths/types of the attacks used by adversaries, it is meaningful to enhance "overall robustness" of models under the worst perturbation ($\text{Acc}_{\text{adv}}^{\max}$). Specifically, our min-max generalized AT leads to 6.27% and 17.63% improvement on S_ϵ compared to single-type AT with ℓ_∞ and ℓ_2 attacks. Furthermore, weighting factor w of the probability simplex helps understand the behavior of AT under mixed types of attacks. Our AMPGD algorithm will adjust w automatically according to the min-max principle - defending the strongest attack. In Figure A2a, as ϵ_{ℓ_2} increases, ℓ_2-attack becomes stronger so its corresponding w increases as well. When $\epsilon_{\ell_2} \geq 2.5$, ℓ_2-attack dominates the adversarial training process. That is to say, our AMPGD algorithm will put more weights on stronger attacks even if the strengths of attacks are unknown, which is a meritorious feature in practice.

(a) weight $\{w_i\}$ **(b)** $\text{Acc}_{\text{adv}}^{\max}$ **(c)** $\text{Acc}_{\text{adv}}^{\text{avg}}$
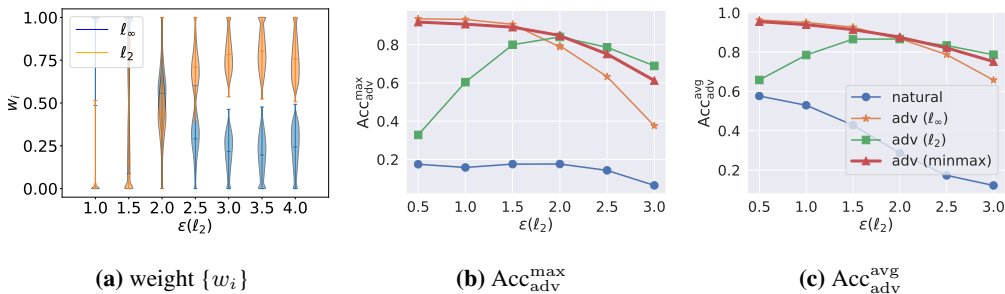
Figure A2: (a): Violin plot of weight w in APGD as a function of perturbation magnitude ϵ of ℓ_2 attack in adversarial training; (b) & (c): Robustness of LeNet (Model C) under different adversarial training schemes.

Table A8 shows complete results on the test accuracy of models in different training schemes. In general, the min-max generalized AT obtains better performance than averaging strategy. AMPGD always leads to Top-2 $\text{Acc}_{\text{adv}}^{\max}$ and $\text{Acc}_{\text{adv}}^{\text{avg}}$.

E.2   COMPARISON WITH UNIVERSAL ADVERSARIAL TRAINING (UAT)

Shafahi et al. (2018) also propose a variant of adversarial training to defend universal perturbations over multiple images. To produce universal perturbations, they propose uSGD to conduct gradient descent on the averaged loss of one-batch images. In consequence, their approach can be regarded as

a variant of our generalized AT in average case. The difference is that they do AT across multiple adversarial images under universal perturbation rather than mixed ℓ_p-norm perturbations.

We added UAT [1] as one of our defense baselines in Table A7. The universal perturbation is generated by uSGD (ℓ_∞ norm, $\epsilon = 0.3$) with a batch size of 128 following Shafahi et al. (2018). We find that a) our proposed approach outperforms UAT under per-image ℓ_p attacks. Taking A7a as an example, our avg and $\min\max$ generalized AT (with DPAR) result in average 17.85% and 17.97% improvement in adversarial test accuracy (ATA), b) our approach has just 3.72% degradation in ATA when encountering universal attacks, and c) both methods yield very similar normal test accuracy. It is not surprising that our average and min-max training schemes can achieve better overall robustness while maintaining competitive performance on defending universal perturbation. This is because the defensed model is trained under more general (ℓ_p norm) and diversity promoted perturbations. As a result, proposed generalized AT is expected to obtain better overall robustness and higher transferability as shown in Table 4 and A7.

Table A7: Adversarial training of MNIST models on single attacks (ℓ_∞ and ℓ_2), multiple attacks ($avg.$ and $\min\max$) and universal perturbation (uni). The perturbation magnitude ϵ for ℓ_∞ and ℓ_2 attacks are 0.2 and 2.0, respectively. uSGD indicates universal adversarial training following Shafahi et al. (2018) (ℓ_∞ norm, $\epsilon = 0.3$). Top 2 test accuracy on each metric are highlighted.

(a) MLP

Opt.	Acc.	Acc-ℓ_∞	Acc-ℓ_2	Acc-uni	Acc$_{adv}^{avg}$
natural	98.30	2.70	13.86	21.61	12.72
ℓ_∞	98.08	**77.70**	69.17	**90.90**	79.26
ℓ_2	98.72	70.03	**81.74**	82.49	78.09
uSGD (ℓ_∞)	98.73	56.21	64.51	**91.27**	70.66
$avg.$	98.62	75.09	79.00	86.69	80.26
+ DPAR	98.50	76.75	79.67	87.88	**81.44**
$\min\max$	98.59	75.96	79.15	86.13	80.41
+ DPAR	98.58	**76.92**	79.74	87.55	**81.40**

(b) LeNet

Opt.	Acc.	Acc-ℓ_∞	Acc-ℓ_2	Acc-uni	Acc$_{adv}^{avg}$
natural	99.25	17.93	39.32	58.93	38.73
ℓ_∞	99.18	**93.80**	78.97	**98.70**	90.49
ℓ_2	99.22	85.84	**87.31**	96.63	89.93
uSGD (ℓ_∞)	99.44	72.81	66.39	**98.37**	79.19
$avg.$	99.22	88.96	85.59	97.41	90.65
+ DPAR	99.25	89.96	**86.49**	97.36	**91.27**
$\min\max$	99.32	89.21	85.98	98.22	91.14
+ DPAR	99.22	**90.19**	86.47	97.77	**91.48**

E.3 OVERLAP OF ℓ_p-NORM BALLS

As reported in Sec. 4.2, our min-max generalized AT does not always result in the best performance on the success rate of defending the worst/strongest perturbation (Acc$_{adv}^{max}$) for given $(\epsilon_{\ell_\infty}, \epsilon_{\ell_2})$ pair, especially when the strengths of two attacks diverge greatly (e.g., ϵ for ℓ_∞ and ℓ_2 attacks are 0.2 and 0.5). In what follows, we provide explanation and analysis about this finding inspired by recent work Araujo et al. (2019).

(a) $\ell_\infty \in \ell_2$ **(b)** $\ell_2 \in \ell_\infty$ **(c)** average ℓ_p-norm
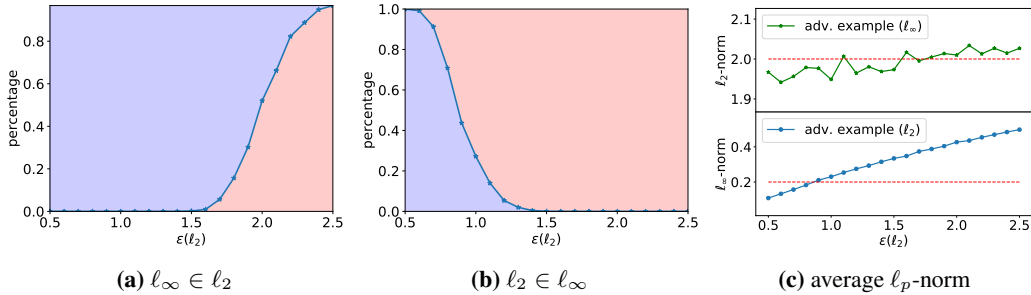
Figure A3: (a) & (b): Comparison of the percentage of adversarial examples inside ℓ_∞ ball (left, blue area) and inside ℓ_2 ball (right, red area). In particular, the red (blue) area in (a) (or (b)) represents the percentage of adversarial examples crafted by ℓ_∞ (ℓ_2) attack that also belong to ℓ_2 (ℓ_∞) ball. We generate adversarial examples on 10,000 test images for each attack. (c): Average ℓ_p norm of adversarial examples as a function of perturbation magnitude ϵ_{ℓ_2}. The top (bottom) side represents the ℓ_2-norm (ℓ_∞) of the adversarial examples generated by ℓ_∞ (ℓ_2) attack as ϵ_{ℓ_2} for generalized AT increases. Note that the same ϵ as the AT procedure is used while attacking trained robust models.

Figure A3 shows the real overlap of ℓ_∞ and ℓ_2 norm balls in adversarial attacks for MLP model on MNIST. Ideally, if ϵ_{ℓ_2} satisfies $\epsilon_{\ell_\infty} < \epsilon_{\ell_2} < \epsilon_{\ell_\infty} \times \sqrt{d}$, ℓ_∞ and ℓ_2 balls will not cover each other

completely Araujo et al. (2019). In other words, AT with ℓ_∞ and ℓ_2 attacks cannot interchange with each other. However, the real range of ϵ_{ℓ_2} for keeping ℓ_2 and ℓ_∞ balls intersected is not $(\epsilon_{\ell_\infty}, \epsilon_{\ell_\infty} \times \sqrt{d})$, because crafted adversarial examples are not uniformly distributed in ℓ_p-norm balls. In Figure A3b, 99.98% adversarial examples devising using ℓ_2 attack are also inside ℓ_∞ ball, even if $0.2 < \epsilon_{\ell_2} = 0.5 < 5.6$. In consequence, AT with ℓ_∞ attack is enough to handle ℓ_2-attack in overwhelming majority cases, which results in better performance than min-max optimization (Table A8a).

Figure A3c presents the average ℓ_p distance of adversarial examples with ϵ_{ℓ_2} increasing. The average ℓ_2-norm (green line) of adversarial examples generated by ℓ_∞ attack remains around 2.0 with a slight rising trend. This is consistent to our setting - fixing ϵ_{ℓ_2} as 0.2. It also indicates model robustness may effect the behavior of attacks - as ϵ_{ℓ_2} increases, robustly trained MLP model becomes more robust against ℓ_2 examples, so the ℓ_∞ attacker implicitly increases ℓ_2 norm to attack the model more effectively. On the other hand, the average ℓ_∞-norm increases substantially as ϵ_{ℓ_2} increases from 0.5 to 2.5. When ϵ_{ℓ_2} arriving at 0.85, the average ℓ_∞ norm gets close to 0.2, so around half adversarial examples generated by ℓ_2-attack are also inside ℓ_∞ balls, which is consistent with Table A3b.

E.4   LEARNING CURVE UNDER DIFFERENT TRAINING SCHEMES

Figure A4 shows the learning curves of model A under different AT schemes, where two setting are plotted: (a) $(\epsilon_{\ell_\infty}, \epsilon_{\ell_2}) = (0.2, 0.5)$; (b) $(\epsilon_{\ell_\infty}, \epsilon_{\ell_2}) = (0.2, 2.0)$. Apart from better worst-case robustness shown in Table A8, our min-max generalized AT leads to a faster convergence compared to average-based AT, especially when the strengths of two attacks diverge greatly. For instance, when $\epsilon_{\ell_2} = 0.5$ (Figure A4a), the robust model trained with AMPGD reaches 70% test accuracy on the worst perturbation (1-$\mathcal{R}_{\text{adv}}^{\max}$) within 210 epochs versus 280 epochs in average setting. When $\epsilon_{\ell_2} = 2.0$ (Figure A4b), the learning curves for min-max and average strategy are very close because the strengths of two attacks are similar, which is verified by approximately equal weights in Figure 3a.

(a) $(\epsilon_{\ell_\infty}, \epsilon_{\ell_2}) = (0.2, 0.5)$ **(b)** $(\epsilon_{\ell_\infty}, \epsilon_{\ell_2}) = (0.2, 2.0)$
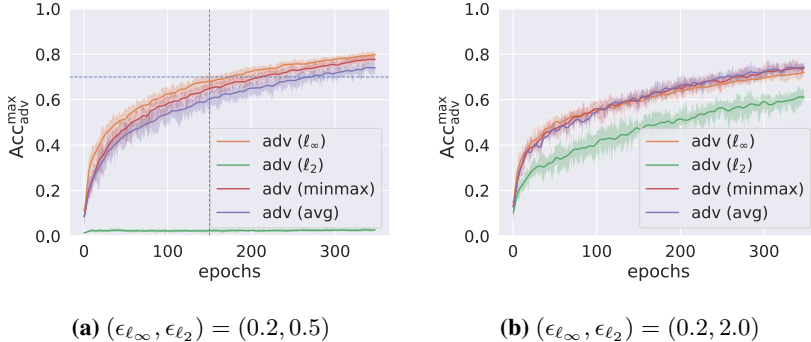
Figure A4: Learning curves of MLP model under different adversarial training schemes on MNIST. Note that each experiment is repeated ten times with different random seeds.

F   INTERPRETABILITY OF DOMAIN WEIGHT w ON UNIVERSAL PERTURBATION TO MULTIPLE IMAGES

Tracking *domain weight* w of the probability simplex from our algorithms is an exclusive feature of solving problem 1. In Sec. 4, we show the strength of w in understanding the procedure of optimization and interpreting the adversarial robustness. Here we would like to show the usage of w in measuring "image robustness" on devising universal perturbation to multiple input samples. Table A9 and A10 show the image groups on MNIST with weight w in APGD and two metrics (distortion of $\ell2$-C&W, minimum ϵ for ℓ_∞-PGD) of measuring the difficulty of attacking single images. The binary search is utilized to searching for the minimum perturbation.

Although adversaries need to consider a trade-off between multiple images while devising universal perturbation, we find that weighting factor w in APGD is highly correlated under different ℓ_p norms. Furthermore, w is also highly related to minimum distortion required for attacking a single image

Table A8: Adversarial training of MNIST models with single attacks (ℓ_∞ and ℓ_2) and multiple attacks ($avg.$ and $\min\max$). During the training process, the perturbation magnitude ϵ_{ℓ_∞} is fixed as 0.2, and ϵ_{ℓ_2} are changed from 0.5 to 3.0 with a step size of 0.5. For min-max scheme, the adversarial examples are crafted using 20-step ℓ_∞-APGD with $\alpha = \frac{1}{6}, \beta = \frac{1}{50}$ and $\gamma = 4$. The ratio of adversarial and benign examples in adversarial training is set as 1.0. For diversity-promoting attack regularizer (DPAR) in generalized AT, the hyperparameter $\lambda = 0.1$.

(a) $(\epsilon_{\ell_\infty}, \epsilon_{\ell_2}) = (0.2, 0.5)$ **(b)** $(\epsilon_{\ell_\infty}, \epsilon_{\ell_2}) = (0.2, 1.0)$

Model	Opt.	Acc.	Acc-ℓ_∞	Acc-ℓ_2	Acc$_{adv}^{max}$	Acc$_{adv}^{avg}$	Acc.	Acc-ℓ_∞	Acc-ℓ_2	Acc$_{adv}^{max}$	Acc$_{adv}^{avg}$
MLP	natural	98.28	2.78	93.75	1.80	48.27	98.30	3.65	72.39	1.17	39.01
	ℓ_∞	98.22	**77.82**	**97.11**	**77.23**	**87.46**	98.29	**78.15**	93.28	**77.95**	**85.71**
	ℓ_2	98.71	12.04	97.10	11.73	54.57	98.98	36.02	94.39	34.68	65.20
	$avg.$	98.83	74.07	97.70	73.67	85.88	98.72	73.97	**94.63**	73.70	84.30
	+ DPAR	98.56	**77.32**	97.74	**76.98**	**87.53**	98.60	76.57	94.41	76.39	85.49
	min max	98.73	75.88	97.43	75.56	86.66	98.72	75.18	94.29	74.92	84.74
	+ DPAR	98.75	77.04	**97.81**	76.72	87.43	98.68	**76.59**	**95.11**	76.49	**85.85**
LeNet	natural	99.17	18.16	97.56	15.23	57.86	9.16	18.24	89.97	15.36	54.10
	ℓ_∞	99.27	**93.60**	98.74	**93.26**	**96.17**	99.28	**93.51**	96.49	**93.13**	**95.00**
	ℓ_2	99.43	34.30	98.49	26.89	66.39	99.50	63.48	96.62	57.94	80.05
	$avg.$	99.29	90.69	**98.89**	90.34	94.79	99.40	89.39	96.94	89.02	93.16
	+ DPAR	99.28	91.81	**98.87**	91.52	**95.34**	99.38	99.09	**97.13**	89.99	93.61
	min max	99.35	90.81	98.74	90.21	94.78	99.31	90.82	**97.20**	90.56	**94.01**
	+ DPAR	99.34	**91.82**	98.77	**91.60**	95.30	99.35	**90.88**	97.07	**90.80**	93.98

(c) $(\epsilon_{\ell_\infty}, \epsilon_{\ell_2}) = (0.2, 1.5)$ **(d)** $(\epsilon_{\ell_\infty}, \epsilon_{\ell_2}) = (0.2, 2.0)$

Model	Opt.	Acc.	Acc-ℓ_∞	Acc-ℓ_2	Acc$_{adv}^{max}$	Acc$_{adv}^{avg}$	Acc.	Acc-ℓ_∞	Acc-ℓ_2	Acc$_{adv}^{max}$	Acc$_{adv}^{avg}$
MLP	natural	98.39	2.77	35.70	2.32	19.23	98.30	2.70	13.86	0.85	8.28
	ℓ_∞	98.34	**78.96**	85.94	**77.42**	82.45	98.08	**77.70**	69.17	66.34	73.43
	ℓ_2	99.00	60.37	**89.96**	59.82	75.16	98.72	70.03	**81.74**	69.14	75.88
	$avg.$	98.61	75.01	88.85	74.76	81.93	98.62	75.09	79.00	72.23	77.05
	+ DPAR	98.68	76.55	88.52	76.18	**82.53**	98.50	76.75	79.67	**74.14**	**78.21**
	min max	98.76	75.66	88.78	75.33	82.22	98.59	75.96	79.15	73.43	77.55
	+ DPAR	98.77	**77.54**	**89.57**	**77.24**	**83.55**	98.58	**76.92**	**79.74**	74.29	**78.35**
LeNet	natural	99.22	14.31	67.69	12.34	41.00	99.25	17.93	39.32	17.57	28.63
	ℓ_∞	99.22	**93.76**	91.11	**90.26**	**92.43**	99.18	**93.80**	78.97	78.80	86.39
	ℓ_2	99.35	79.92	93.27	77.39	86.60	99.22	85.84	**87.31**	84.06	86.58
	$avg.$	99.31	89.26	**93.29**	88.77	91.28	99.22	88.96	85.59	84.29	87.28
	+ DPAR	99.27	**90.75**	93.48	**89.96**	**92.11**	99.25	89.96	**86.49**	85.44	**88.23**
	min max	99.40	89.83	92.96	89.00	91.39	99.32	89.21	85.98	84.82	87.60
	+ DPAR	99.35	90.64	93.27	89.80	91.96	99.22	**90.19**	86.47	**85.47**	**88.33**

(e) $(\epsilon_{\ell_\infty}, \epsilon_{\ell_2}) = (0.2, 2.5)$ **(f)** $(\epsilon_{\ell_\infty}, \epsilon_{\ell_2}) = (0.2, 3.0)$

Model	Opt.	Acc.	Acc-ℓ_∞	Acc-ℓ_2	Acc$_{adv}^{max}$	Acc$_{adv}^{avg}$	Acc.	Acc-ℓ_∞	Acc-ℓ_2	Acc$_{adv}^{max}$	Acc$_{adv}^{avg}$
MLP	natural	98.31	3.37	6.02	2.27	4.70	98.24	2.92	2.42	1.54	2.67
	ℓ_∞	98.25	**77.91**	51.28	49.40	64.59	98.35	**79.15**	32.58	31.23	55.86
	ℓ_2	98.10	73.94	**70.01**	**67.66**	**71.97**	97.55	73.86	**58.24**	**57.83**	**66.05**
	$avg.$	98.47	75.35	64.39	63.37	69.86	98.17	75.07	49.75	49.49	62.41
	+ DPAR	98.18	76.33	**66.49**	65.54	71.41	97.85	74.61	**51.16**	**51.04**	62.89
	min max	98.44	75.48	66.12	64.99	70.80	98.10	74.71	50.45	50.54	62.58
	+ DPAR	98.20	**76.98**	66.42	**65.55**	**71.70**	97.97	**76.13**	51.12	51.00	**63.63**
LeNet	natural	99.23	15.25	16.08	11.16	15.67	99.24	13.76	4.74	2.57	9.25
	ℓ_∞	99.18	**94.09**	60.18	58.47	77.13	99.30	**93.14**	39.48	32.93	65.81
	ℓ_2	98.94	87.57	**78.45**	**78.42**	**83.01**	98.55	87.87	**68.69**	**68.34**	**78.28**
	$avg.$	99.10	89.88	74.68	74.39	82.28	99.10	89.19	59.87	60.01	74.53
	+ DPAR	99.14	**90.17**	75.16	75.09	**82.67**	98.95	**89.80**	62.21	61.19	75.50
	min max	99.21	88.88	74.97	74.42	81.93	99.01	88.93	61.15	60.76	75.04
	+ DPAR	99.09	89.34	**75.55**	**75.45**	82.45	98.98	89.53	**63.22**	**63.18**	**76.37**

successfully. It means the inherent "image robustness" exists and effects the behavior of generating universal perturbation. Larger weight w usually indicates an image with higher robustness (e.g., fifth 'zero' in the first row of Table A9), which usually corresponds to the MNIST letter with clear appearance (e.g., bold letter).

Table A9: Interpretability of domain weight w for universal perturbation to multiple inputs on MNIST (*Digit 0 to 4*). Domain weight w for different images under ℓ_p-norm ($p = 0, 1, 2, \infty$) and two metrics measuring the difficulty of attacking single image are recorded, where dist. (ℓ_2) denotes the the minimum distortion of successfully attacking images using C&W (ℓ_2) attack; $\epsilon_{\min}$ (ℓ_∞) denotes the minimum perturbation magnitude for ℓ_∞-PGD attack.

	Image										
Weight	ℓ_0	0.	0.	0.	0.	1.000	0.248	0.655	0.097	0.	0.
	ℓ_1	0.	0.	0.	0.	1.000	0.07	0.922	0.	0.	0.
	ℓ_2	0.	0.	0.	0.	1.000	0.441	0.248	0.156	0.155	0.
	ℓ_∞	0.	0.	0.	0.	1.000	0.479	0.208	0.145	0.168	0.
Metric	dist.(C&W ℓ_2)	1.839	1.954	1.347	1.698	3.041	1.545	1.982	2.178	2.349	1.050
	$\epsilon_{\min}$ (ℓ_∞)	0.113	0.167	0.073	0.121	0.199	0.167	0.157	0.113	0.114	0.093

	Image										
Weight	ℓ_0	0.	0.	0.613	0.180	0.206	0.	0.	0.223	0.440	0.337
	ℓ_1	0.	0.	0.298	0.376	0.327	0.	0.	0.397	0.433	0.169
	ℓ_2	0.	0.	0.387	0.367	0.246	0.	0.242	0.310	0.195	0.253
	ℓ_∞	0.087	0.142	0.277	0.247	0.246	0.	0.342	0.001	0.144	0.514
Metric	dist.(C&W ℓ_2)	1.090	1.182	1.327	1.458	0.943	0.113	1.113	1.357	1.474	1.197
	$\epsilon_{\min}$ (ℓ_∞)	0.075	0.068	0.091	0.105	0.096	0.015	0.090	0.076	0.095	0.106

	Image										
Weight	ℓ_0	0.	1.000	0.	0.	0.	0.	0.	0.909	0.	0.091
	ℓ_1	0.	1.000	0.	0.	0.	0.	0.	0.843	0.	0.157
	ℓ_2	0.	0.892	0.	0.	0.108	0.	0.	0.788	0.	0.112
	ℓ_∞	0.	0.938	0.	0.	0.062	0.	0.	0.850	0.	0.150
Metric	dist.(C&W ℓ_2)	1.335	2.552	2.282	1.229	1.884	1.928	1.439	2.312	1.521	2.356
	$\epsilon_{\min}$ (ℓ_∞)	0.050	0.165	0.110	0.083	0.162	0.082	0.106	0.176	0.072	0.171

	Image										
Weight	ℓ_0	0.481	0.	0.378	0.	0.	0.	0.352	0.	0.	0.648
	ℓ_1	0.690	0.	0.310	0.	0.	0.	0.093	0.205	0.	0.701
	ℓ_2	0.589	0.069	0.208	0.	0.134	0.064	0.260	0.077	0.	0.600
	ℓ_∞	0.864	0.	0.084	0.	0.052	0.079	0.251	0.156	0.	0.514
Metric	dist.(C&W ℓ_2)	2.267	1.656	2.053	1.359	0.861	1.733	1.967	1.741	1.031	2.413
	$\epsilon_{\min}$ (ℓ_∞)	0.171	0.088	0.143	0.117	0.086	0.100	0.097	0.096	0.038	0.132

	Image										
Weight	ℓ_0	0.	0.	0.753	0.	0.247	0.	0.	0.	1.000	0.
	ℓ_1	0.018	0.	0.567	0.	0.416	0.347	0.	0.	0.589	0.063
	ℓ_2	0.	0.	0.595	0.	0.405	0.346	0.	0.	0.654	0.
	ℓ_∞	0.	0.	0.651	0.	0.349	0.239	0.	0.	0.761	0.
Metric	dist.(C&W ℓ_2)	1.558	1.229	1.939	0.297	1.303	0.940	1.836	1.384	1.079	2.027
	$\epsilon_{\min}$ (ℓ_∞)	0.084	0.088	0.122	0.060	0.094	0.115	0.103	0.047	0.125	0.100

Table A10: Interpretability of domain weight w for universal perturbation to multiple inputs on MNIST (*Digit 5 to 9*). Domain weight w for different images under ℓ_p-norm ($p = 0, 1, 2, \infty$) and two metrics measuring the difficulty of attacking single image are recorded, where dist. (ℓ_2) denotes the the minimum distortion of successfully attacking images using C&W (ℓ_2) attack; $\epsilon_{\min}$ (ℓ_∞) denotes the minimum perturbation magnitude for ℓ_∞-PGD attack.

Image											
Weight	ℓ_0	0.	0.062	0.254	0.	0.684	0.457	0.	0.	0.542	0.
	ℓ_1	0.131	0.250	0.	0.	0.619	0.033	0.157	0.005	0.647	0.158
	ℓ_2	0.012	0.164	0.121	0.	0.703	0.161	0.194	0.	0.508	0.136
	ℓ_∞	0.158	0.008	0.258	0.	0.576	0.229	0.179	0.	0.401	0.191
Metric	dist. (ℓ_2)	1.024	1.532	1.511	1.351	1.584	1.319	1.908	1.020	1.402	1.372
	$\epsilon_{\min}$ (ℓ_∞)	0.090	0.106	0.085	0.069	0.144	0.106	0.099	0.0748	0.131	0.071

Image											
Weight	ℓ_0	0.215	0.	0.	0.194	0.590	0.805	0.	0.	0.195	0.
	ℓ_1	0.013	0.	0.	0.441	0.546	0.775	0.	0.	0.225	0.
	ℓ_2	0.031	0.	0.	0.410	0.560	0.767	0.	0.	0.233	0.
	ℓ_∞	0.	0.	0.	0.459	0.541	0.854	0.	0.	0.146	0.
Metric	dist. (ℓ_2)	1.199	0.653	1.654	1.156	1.612	2.158	0.	1.063	1.545	0.147
	$\epsilon_{\min}$ (ℓ_∞)	0.090	0.017	0.053	0.112	0.158	0.159	0.020	0.069	0.145	0.134

Image											
Weight	ℓ_0	0.489	0.	0.	0.212	0.298	0.007	0.258	0.117	0.482	0.136
	ℓ_1	0.525	0.190	0.	0.215	0.070	0.470	0.050	0.100	0.343	0.038
	ℓ_2	0.488	0.165	0.	0.175	0.172	0.200	0.175	0.233	0.378	0.014
	ℓ_∞	0.178	0.263	0.	0.354	0.205	0.258	0.207	0.109	0.426	0.
Metric	dist. (ℓ_2)	1.508	1.731	1.291	1.874	1.536	1.719	2.038	1.417	2.169	0.848
	$\epsilon_{\min}$ (ℓ_∞)	0.110	0.125	0.089	0.126	0.095	0.087	0.097	0.084	0.135	0.077

Image											
Weight	ℓ_0	0.	0.	1.000	0.	0.	0.246	0.	0.	0.	0.754
	ℓ_1	0.	0.180	0.442	0.378	0.	0.171	0.	0.	0.	0.829
	ℓ_2	0.	0.298	0.593	0.109	0.	0.330	0.	0.	0.	0.670
	ℓ_∞	0.	0.377	0.595	0.028	0.	0.407	0.	0.	0.	0.593
Metric	dist. (ℓ_2)	1.626	1.497	1.501	1.824	0.728	1.928	1.014	1.500	1.991	1.400
	$\epsilon_{\min}$ (ℓ_∞)	0.070	0.153	0.156	0.156	0.055	0.171	0.035	0.090	0.170	0.161

Image											
Weight	ℓ_0	1.	0.	0.	0.	0.	0.	0.665	0.331	0.	0.004
	ℓ_1	0.918	0.	0.012	0.	0.070	0.	0.510	0.490	0.	0.
	ℓ_2	0.911	0.	0.089	0.	0.	0.	0.510	0.490	0.	0.
	ℓ_∞	0.935	0.	0.065	0.	0.	0.	0.665	0.331	0.	0.004
Metric	dist. (ℓ_2)	1.961	1.113	1.132	1.802	0.939	1.132	1.508	1.335	1.033	1.110
	$\epsilon_{\min}$ (ℓ_∞)	0.144	0.108	0.083	0.103	0.079	0.041	0.090	0.103	0.083	0.044